

See discussions, stats, and author profiles for this publication at: <https://www.researchgate.net/publication/351245869>

English Technical Report and Correction: Performance Comparison of SMC, LQR and PD control for Spacecraft High Accuracy Pointing (Teilvorhaben TU Braunschweig)

Technical Report · May 2021

DOI: 10.13140/RG.2.2.20358.50247

CITATIONS

0

READS

156

1 author:



Divya Bhatia

The American Institute of Aeronautics and Astronautics

28 PUBLICATIONS 64 CITATIONS

SEE PROFILE

Some of the authors of this publication are also working on these related projects:



Attitude Control System of Sub-Arcsec Pointing Spacecraft [View project](#)



InfraRed Astronomy Satellite Swarm Interferometer (IRASSI) Mission [View project](#)

Final Technical Report: Infrared Astronomy Satellite Swarm Interferometry (IRASSI)-2 Phase-1

Performance Comparison of SMC, LQR and PD control for Spacecraft High Accuracy Pointing

**FKZ 50NA1715
(Teilvorhaben TU Braunschweig)**

Grant Recipients:
Technische Universität Braunschweig
Pockelsstraße 14
D-38106 Braunschweig

Executing Agency:
Technische Universität Braunschweig
Institut für Flugführung
Hermann-Blenk-Str. 27
D-38108 Braunschweig

Name	Institution	Date	Comments
------	-------------	------	----------

Author(s):

Divya Bhatia (Technical Report and German Translation)	IFF	10/12/2018	

Contributor(s):

Yannic Beyer (German Translation correction)	IFF		
--	-----	--	--

Distribution Record

Internal	External
Meiko Steen	

Table of Contents

Inhalt

1. INTRODUCTION	8
2. IRASSI TEAM MEMBERS	10
3. PROJECT PLANNING AND EXECUTION	12
4. CLOSED-LOOP FEEDBACK CONTROL METHODOLOGY	13
5. REFERENCE FRAMES REQUIRED FOR IRASSI SPACECRAFT ATTITUDE CONTROL.....	17
6. SPACECRAFT ROTATIONAL EQUATIONS OF MOTION	18
7. IRASSI SPACECRAFT EXTERNAL DISTURBANCES.....	21
7.1. Gravity-Gradient Torque.....	21
7.2. Constant External Torque	22
8. SLIDING MODE CONTROL (SMC)	23
8.1. Methodology	23
8.2. Simulation Results	24
9. LINEAR QUADRATIC REGULATOR (LQR)	30
9.1. Methodology	30
9.2. Simulation Results	31
10. LINEAR AND NONLINEAR PROPORTIONAL-DERIVATIVE (PD) CONTROL.....	34
10.1. Methodology	34
10.2. Simulation Results	34
11. CLOSED LOOP STABILITY OF NONLINEAR CONTROL ALGORITHMS	41
11.1. Lyapunov Direct Method.....	41
11.2. Linear/linearized system stability conditions.....	41
11.3. Nonlinear PD Stability Proof.....	41
11.4. LQR Stability Proof.....	42
11.5. SMC Stability Proof.....	42
12. PERFORMANCE COMPARISON AND ANALYSIS OF CONTROL ALGORITHMS	44
13. SOFTWARE ENVIRONMENT FOR SPACECRAFT CONTROL IMPLEMENTATION.....	45
14. CONCLUSION	46

15.	COOPERATION WITH PARTNERS	47
16.	APPLICATION	48
17.	IMPLEMENTATION.....	49
17.1.	Publication.....	49
17.2.	Promotion of IRASSI to Space Agencies	49
17.3.	Students & Teaching	49
18.	BIBLIOGRAPHY	50
19.	CORRECTION.....	51

Index of figures

Figure 1 a. Attitude Definitions: Pointing Error(PE), Measurement Error (ME) and Control Error (CE). b. IRASSI Spacecraft showing spacecraft fixed-reference frame and the position-orientation of attitude and inertial sensors [2], [3].	10
Figure 2 Workpackage of Technische Universitaet Braunschweig (AP5).	11
Figure 3 Time plan for Workpackage 5 for Attitude Control system.	12
Figure 4 Attitude Determination and Control System.	14
Figure 5 Feedback Closed-Loop Attitude Control Block diagram.	15
Figure 6 Stable and Unstable equilibria corresponding to the continuous feedback control law using the rotation matrix and unit quaternion. Extracted from [9].	19
Figure 7 Unwinding Phenomenon depiction. Figure extracted from [9].	20
Figure 8 Gravity-gradient torque on rigid spacecraft in restricted three-body problem. Extracted from [7].	21
Figure 9 Solar Radiation Pressure cases.	22
Figure 10 Sliding Mode Control depicting the sliding surface, chattering and two phases namely reaching and sliding phase.	23
Figure 11 Large Angle Slew case 1: a. Quaternion Tracking b. Angular velocity Tracking.	25
Figure 12 Large Angle Slew case 1: a. Quaternion Errors b. Control Torques.	26
Figure 13 Large Angle Slew case 1: a. Sliding Surface b. Phase Plots.	26
Figure 14 Large Angle Slew case 2: a. Quaternion Tracking b. Angular velocity Tracking.	27
Figure 15 Large Angle Slew case 2: a. Quaternion Errors b. Control Torques.	27
Figure 16 Large Angle Slew case 2: a. Sliding Surface b. Phase Plots.	28
Figure 17 Small Angle Slew: a. Quaternion Tracking b. Angular velocity Tracking.	28
Figure 18 Small Angle Slew: a. Quaternion Errors b. Control Torques.	28
Figure 19 Small Angle Slew: a. Sliding Surface b. Phase Plots.	29
Figure 20 LQR Large Angle Maneuver Case 1 a. Quaternion and Angular Velocity Tracking b. Control Torques and Quaternion errors.	32
Figure 21 LQR Large Angle Maneuver Case 2 a. Quaternion and Angular Velocity Tracking b. Control Torques and Quaternion errors.	32
Figure 22 LQR Small Angle Maneuver Case 1 a. Quaternion and Angular Velocity Tracking b. Control Torques and Quaternion errors.	33
Figure 23 LQR Small Angle Maneuver Case 2 a. Quaternion and Angular Velocity Tracking b. Control Torques and Quaternion errors.	33
Figure 24 Linear PD: a. Large angle slew: Quaternion and Angular velocity Tracking b. Small angle slew: Quaternion and Angular velocity Tracking.	35
Figure 25 Linear PD- Large angle slew a. Control Torques when Quaternion errors~0.02 arcsec b. Control Torques when Quaternion errors~0.05 arcsec.	36
Figure 26 Linear PD- Small angle slew a. Control Torques when Quaternion errors~0.02 arcsec b. Control Torques when Quaternion errors~0.05 arcsec.	36
Figure 27 Negative NonLinear PD: a. Large angle slew: Quaternion and Angular velocity Tracking b. Small angle slew: Quaternion and Angular velocity Tracking.	37
Figure 28 Negative Nonlinear PD- Large angle slew a. Control Torques when Quaternion errors~0.02 arcsec b. Control Torques when Quaternion errors~0.05 arcsec.	37

Figure 29 Negative Nonlinear PD- Small angle slew a. Control Torques when Quaternion errors~0.02 arcsec b. Control Torques when Quaternion errors~0.05 arcsec.	38
Figure 30 Positive NonLinear PD: a. Large angle slew: Quaternion and Angular velocity Tracking b. Small angle slew: Quaternion and Angular velocity Tracking.	38
Figure 31 Positive Nonlinear PD- Large angle slew a. Control Torques when Quaternion errors~0.02 arcsec b. Control Torques when Quaternion errors~0.05 arcsec.	39
Figure 32 Positive Nonlinear PD- Small angle slew a. Control Torques when Quaternion errors~0.02 arcsec b. Control Torques when Quaternion errors~0.05 arcsec.	39
Figure 33 Architecture of MATLAB Simulation environment.	45

Index of tables

Table 1 Scientific and Engineering Requirements for IRASSI [1].	9
Table 2 Status of Workpackages for AP5 Attitude Control System.	12
Table 3 Comparison of Nonlinear and Linear Control systems.	16
Table 4 Accuracies Achieved by SMC Cases.	28
Table 5 Accuracies Achieved by LQR Cases.	33
Table 6 Characteristics of PD control corresponding to its gains.	34
Table 7 Accuracies Achieved by Linear and NL PD controllers.	39
Table 8 Approximate maximum control torques applied for achieving accuracies ≤ 0.05 arcsec by SMC, LQR and PD controllers.	40
Table 9 Performance Comparison of SMC, PD and LQR control design for IRASSI Spacecraft attitude tracking rest-to-rest maneuvers.	44
Table 10 IRASSI Spacecraft Pointing Accuracies Achieved By Attitude Navigation (IRASSI 1) and Control Systems (IRASSI 2 Phase 1).	46
Table 11 Controllers corresponding to the two IRASSI mission modes defined in IRASSI 1.	46

1. INTRODUCTION

IRASSI is an interferometry mission consisting of a 3D swarm of 5 telescopes orbiting the Sun-Earth Lagrange point 2 in a halo orbit orbit. The scientific goal of this mission is to map the circumstellar disks and protoplanetary areas where the formation of stars and planets takes place. These processes are visible only in the Far-InfraRed (FIR) region of the electromagnetic (EM) field. To study these processes, high-quality images with an angular resolution of less than 1 arc second are required, which provides a constraint on the pointing accuracy of IRASSI telescopes. This requirement was determined together with the other scientific and engineering requirements by the Max Planck Institute for Astronomy, Heidelberg, as in Table 1 [1].

IRASSI telescopes are single receivers, i.e., the focal plane of each telescope is not filled with detector elements, but has only one receiver horn which collects the signals from the sources being studied. The final visibility functions are constructed by correlating the signals of all telescopes. The main lobe of the power spectrum provides the highest sensitivity for uniform exposure of the main dish. Since the telescope's high power spectrum has a reciprocal relationship to the diameter of the telescope, the need for pointing accuracy depends on the upper frequency range of the operating FIR spectrum of IRASSI. i.e., at 6 THz. At this frequency, the width of the half power beam width (HPBW) of the main lobe is minimal. This results in a stringent absolute pointer error (APE) requirement of each satellite of at least 0.4 arc seconds and the target of 0.2 arc seconds, so that the target is within one-tenth of the HPBW of each telescope. This APE requirement should be achieved after the estimation and control of the IRASSI telescopes.

A High Accuracy Attitude Determination Estimation System (ADES) [2], [3], [4] was designed in IRASSI 1 by AP5 that achieved a worst-case accuracy of 0.1 arcsec and a best-case accuracy of 0.04 arcsec. IRASSI 1 also led to the placement (position and orientation) of the IRASSI sensors onboard IRASSI spacecraft, as shown in Figure 1b. In IRASSI 2 phase 1, we develop control algorithms for IRASSI spacecraft attitude control that achieves a pointing accuracy <0.3 arcsec. Hence, the total pointing accuracy from the complete Attitude Determination Control System (ADCS) (theoretically, shown in Figure 4) of IRASSI is < 0.4 arcsec and equal to 0.2 arcsec (best-case) for some control algorithms as shown in sections below. This leads to achieving the imposed total pointing accuracy requirement on IRASSI spacecraft (Table 1 [1]). This also leaves enough margin for pointing errors (as shown in Figure 1a) due to IRASSI spacecraft reaction wheels (required for attitude slews and part of ongoing IRASSI 2 phase 2 work), thruster firing (used for IRASSI formation control), cryogenic coolers, propellant sloshing and other structural instabilities, to name a few. Figure 1a shows that Absolute Pointing Error (PE) is composed of Measurement Error (ME) and Control Error (CE).

This document describes the work carried out by the Institute of Flight Guidance (IFF) at Technical University of Braunschweig (TUBS) in the research project titled "IRASSI". IFF was responsible for the work package 5 "Attitude Control System", which was divided in two sub-work packages and included the development of attitude control algorithms of IRASSI satellites. Pertaining to this, three attitude control algorithms were investigated, which were modified for IRASSI spacecraft because IRASSI is exposed to two external disturbance torques in its halo orbit around lagrange point L2, i.e. gravity-gradient torque and solar radiation pressure torque. An additional constant torque was also added to account for any unforeseen disturbances. These algorithms include linear (PD and LQR) and non-linear controls (PD and SMC); and are applied to nonlinear spacecraft rotational equations of motion. Stability of these controllers are established via Lyapunov Theory. Performance of these controllers are compared based on the pointing accuracy achieved by them, their global stability and their robustness towards external disturbances, initial conditions and large angle slews.

Field	Required value
Number of Telescopes	5
Number of baselines	10 (baseline number = $\frac{N(N-1)}{2}$)
Size of telescop mirrors	3.5 m primary mirror
Satellite configuration	Free-flying 3D
Length of baselines	7-850 m
Wavelength range	50-300 μm
Frequency range	1-6 THz
Field of View (of each telescope)	3-18 arcsec (Depends on frequency)
Telescope Pointing Accuracy	0.4 arcsec (Requirement), 0.2 arcsec (goal)
Accuracy of satellite distances	5 μm (in all directions)

Table 1 Scientific and Engineering Requirements for IRASSI [1].

2. IRASSI TEAM MEMBERS

TU Braunschweig is a partner in the IRASSI collaboration project and is the beneficiary of 100% funding by the space management of the German Aerospace Center (DLR, Bonn) via funds from the Federal Ministry for Economic Affairs and Energy on the basis of a resolution of the German Bundestag. The following project partners were involved in the overall project:

- Menlo Systems GmbH (Project Manager)
- Max-Planck-Institut für Astronomie
- Universität der Bundeswehr München
- Technische Universität Braunschweig

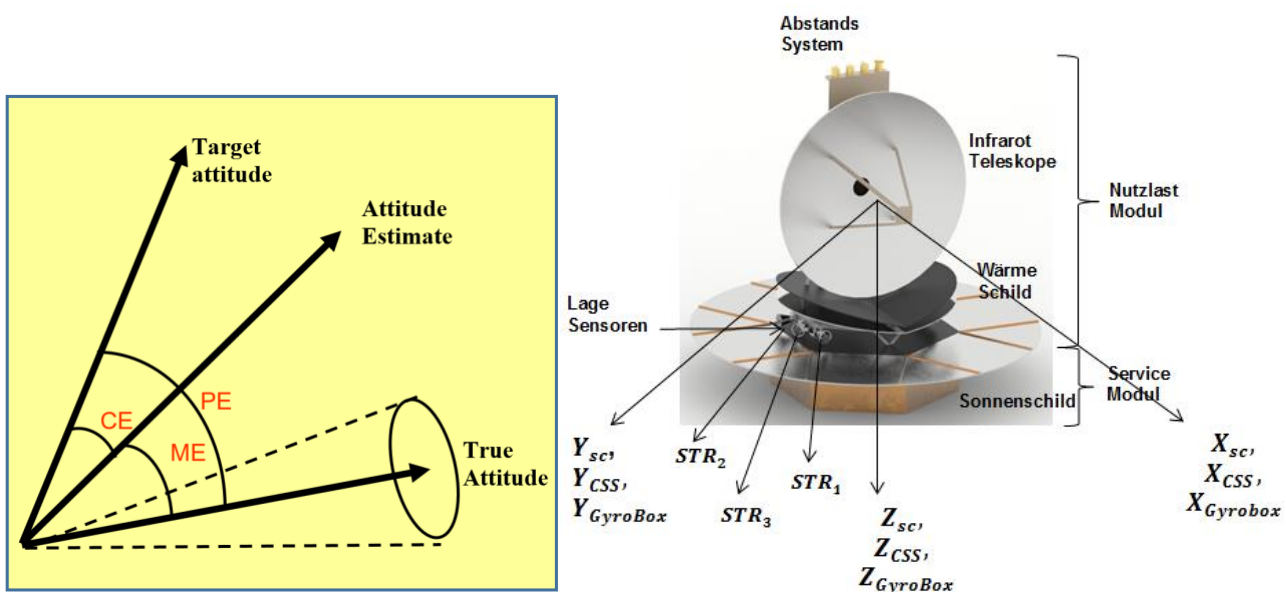


Figure 1 a. Attitude Definitions: Pointing Error(PE), Measurement Error (ME) and Control Error (CE). b. IRASSI Spacecraft showing spacecraft fixed-reference frame and the position-orientation of attitude and inertial sensors [2], [3].

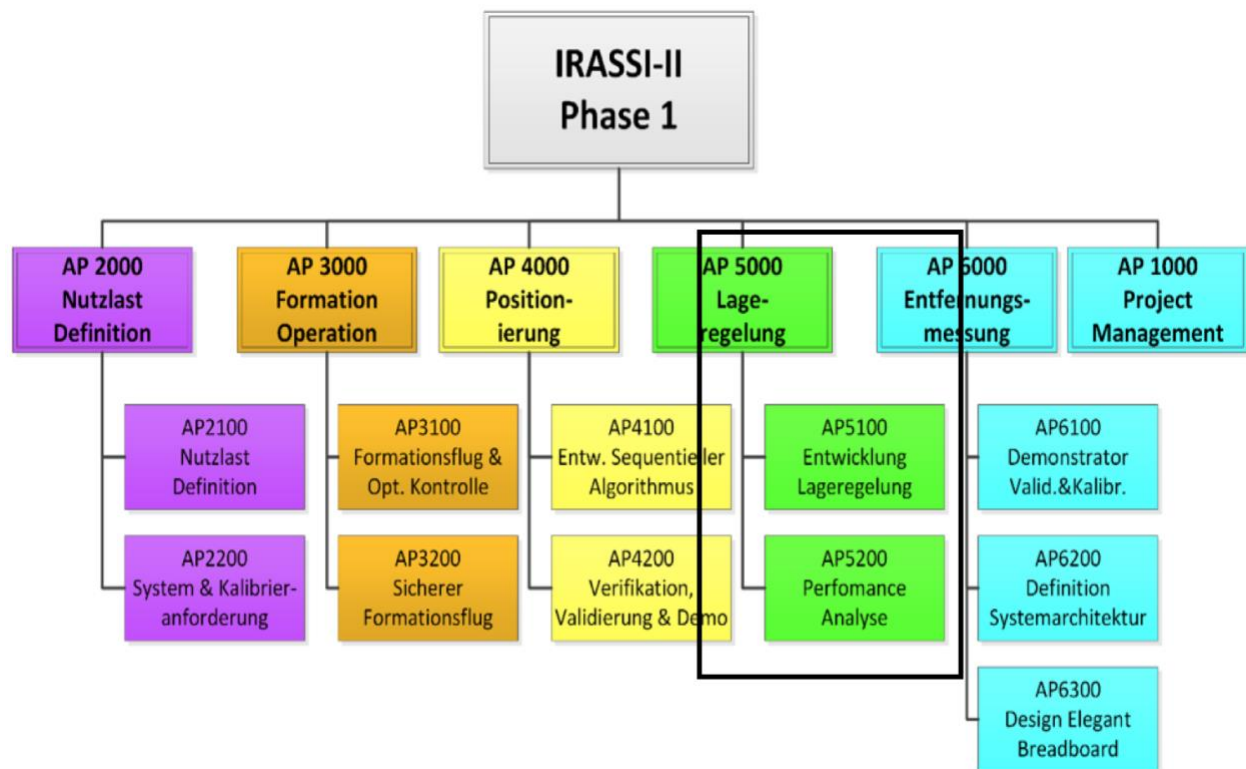


Figure 2 Workpackage of Technische Universitaet Braunschweig (AP5).

3. PROJECT PLANNING AND EXECUTION

IFF at TU-Braunschweig was responsible for the main work package 5. For HAP 5, two sub-work packages were determined, namely AP 5.1 - AP 5.2, as shown in Figure 2 and Table 2. Figure 3 shows the schedule for each work package. Both AP 5.1 and AP 5.2 each lasted about six months and ended on time as shown in Table 2.

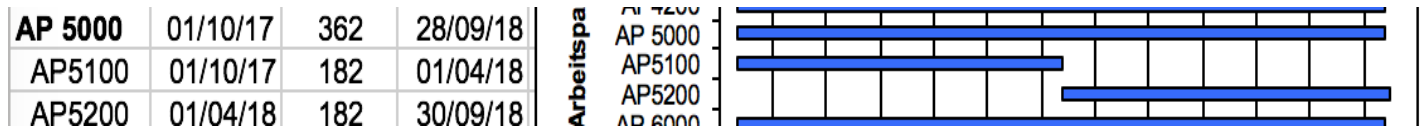


Figure 3 Time plan for Workpackage 5 for Attitude Control system.



AP5 Attitude Control System	Status	Status
5.1 Attitude Control Algorithmus Development		(In Time) ✓
5.2 Attitude Control System Performance Analysis		(In Time) ✓

Table 2 Status of Workpackages for AP5 Attitude Control System.

4. CLOSED-LOOP FEEDBACK CONTROL METHODOLOGY

The work in this section is carried out within sub-work package 5.1. Attitude control comprises of the 1. maintenance of the current attitude and 2. re-orientation to another desired attitude by commanding the actuators to apply torques based on the current attitude information from the sensors and desired attitude specification from the guidance. It is one part of the “Attitude Determination and Control System” (the other part being Attitude Determination which was the work of IRASSI 1) as shown in Figure 4. For IRASSI, the main role of Attitude Control System is in maintaining a high accuracy pointing to a specified target during the science mode of the mission with an accuracy of ≤ 0.3 arcsec.

The constituents of complete ADCS are Attitude Determination and Estimation system (ADES, developed in IRASSI 1 [4]) and the Attitude Control System (ACS, developed in IRASSI 2 phase 1). The role of the ACS is to control the orientation of a spacecraft throughout all its mission stages. Various activities include:

- Acquisition (where the attitude determination system derives the first estimate of the attitude and rotation rates), when the attitude control system starts to reduce rotation rates in order to stabilize pointing and achieve an inertial lock during the mission operations.
- Attitude Regulation: Reference [5] defines Regulation control as bringing the attitude to some fixed location (usually identity quaternion) and angular velocity to zero. For IRASSI science mission operation, a fine regulation pointing of accuracy ≤ 0.3 arcsec is required. Fine pointing is where the IRASSI satellites are fully inertial-stabilized to allow precise pointing for science observations. This type of control leads to a maneuverer called as Rest-to-Rest maneuverer.
- Attitude Tracking: Reference [5] defines Tracking control as following any form of time-varying trajectory with varying desired quaternion and varying desired angular velocity. This also encompasses the case of Regulation with desired attitude set to a constant quaternions and desired angular velocity set to zero. For IRASSI, ideal Attitude Tracking where both desired angular velocity and angles are varying is not required. Only Rest-to-rest slew manoeuvres are required for IRASSI, where once pointing is set to one scientific target, it is observed for one observation cycle, i.e. nearly 22 hours.

Spacecraft attitude control development involves control algorithms that 1. reorients the attitude from one orientation to next (called as Tracking) and 2. Maintains orientation to a certain specific target for observations (called as Regulation). For IRASSI, it is demanded from ACS to maintain an attitude regulation with an accuracy of ≤ 0.3 arcsec during science observations phase. For this purpose, control algorithms are developed in a feedback form where the output from the plant/system (equations of motion) are included in the controller which enables the system to adjust its performance to meet a desired output response as shown in Figure 5. The plant in Figure 5 are the equations of motion of the system (for our case, spacecraft) or can be the error equations of motion of the system (as in LQR shown in Section 9). Hence, one can transcribe between a full-state feedback control system or an error state feedback control system. Once a controller has been analytically designed, the task is to determine the feedback gain ‘K’ such that the error between the real plant out and the desired/reference output approaches to zero (this condition makes the system “stable”, as also explained in the Lyapunov theorem in Section 11).

Real dynamic systems (spacecraft, aircraft, UAVs, cars etc.) encounter real-life conditions in which they are operating under internal and external disturbances and model uncertainties. For IRASSI spacecraft ACS, two external disturbances affecting it in its Halo orbit around Lagrange point 2 are gravity-gradient torque and the solar radiation pressure which are feed-forwarded to the spacecraft plant described by its equations of motion for the determination of the control as shown in the Figure 5. Hence the controller that is developed for IRASSI spacecraft needs to take into account the effect of these two disturbances acting on it and achieve the stringent pointing accuracy. These disturbances acting on the IRASSI spacecraft are detailed in Section 7 below.

Many control algorithms have been developed and documented in literature for spacecraft attitude control like straightforward Proportional-Derivative (PD) (linear and nonlinear) control, backstepping control, robust control like Sliding Mode Control (SMC), adaptive control, Nonlinear Dynamic Inversion control etc. All the control algorithms can be divided into categories depending on whether they are optimal or not, robust or not, adaptive or not, model dependent or model-independent, linear or nonlinear control, for linear/linearized system or nonlinear systems depending on how they are developed. For our

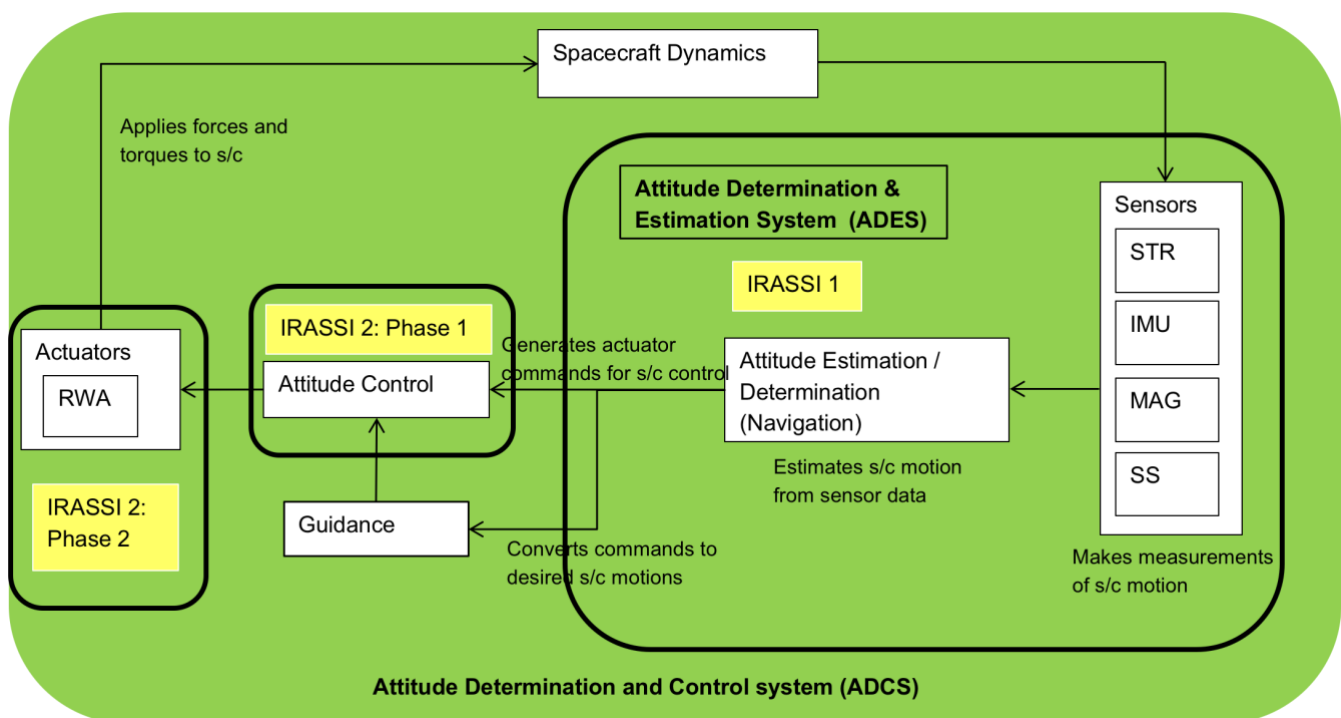


Figure 4 Attitude Determination and Control System.

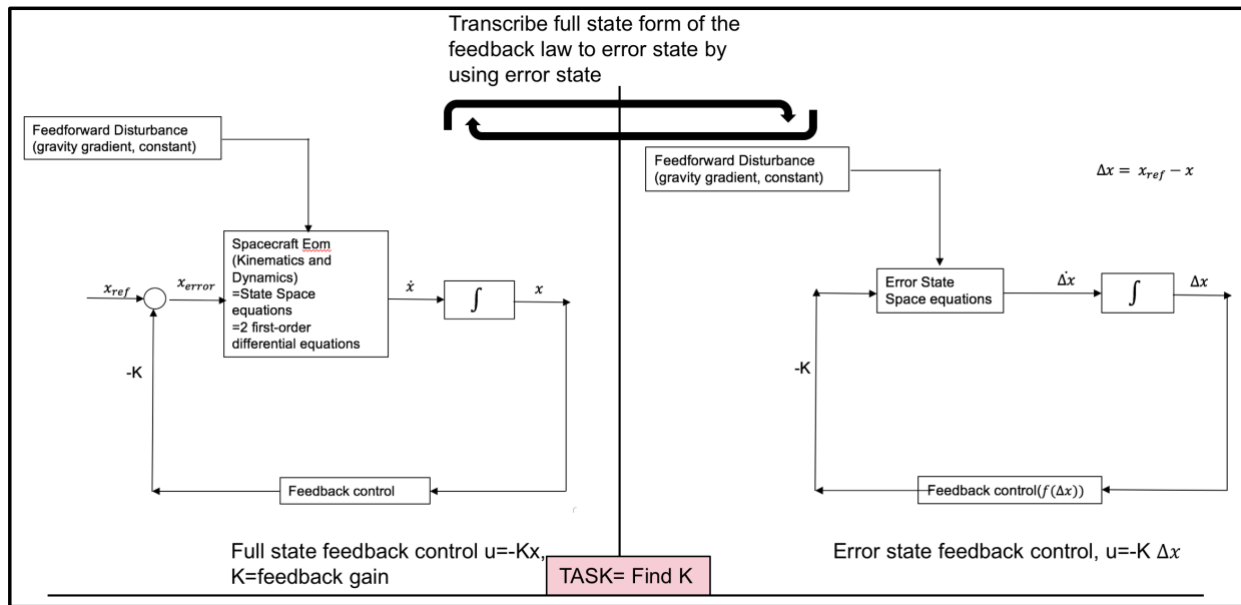


Figure 5 Feedback Closed-Loop Attitude Control Block diagram.

study we looked at three different controllers, i.e. PD (Linear and nonlinear control) for Nonlinear Spacecraft Equations of motion (as described in Section 10), Linear Quadratic Regulator (LQR) (requires linear/linearized system equations of motion as described in Section 9) and SMC (for nonlinear system and is theoretically robust towards disturbances and model uncertainties as described in Section 8). These three controllers have their own characteristics with advantages and disadvantages which are detailed in the sections below.

Performance characteristics of these controllers include their stability (global or local), finite-time convergence and robustness towards external/internal disturbances, uncertainties in the system modeling, large or small slews and initial conditions. Another performance is their adaptivity to real-time varying conditions in which the system is operating in. For IRASSI, adaptivity is out of scope due to time restriction. In this research, we compare linear and nonlinear controllers based on these performance indices as listed in Table 3, which shows that nonlinear systems and controls provide global control over linear/linearized control. NL control is suitable for arbitrary changes to spacecraft attitude which is not really the case for linear controls. NL control is also robust towards initial conditions unlike linear controls. Finally, NL system represents the actual system whereas linear systems only represent an approximate system which is not sufficient for solving Spacecraft attitude control problem where we want to maximize the performance of the controllers since no human intervention is possible at Lagrange point 2 (IRASSI spacecraft operating place/environment). Hence the work done in [6] is severely insufficient where the spacecraft equations of motion are linearized including the gravity gradient torque equation. Additionally, the additive quaternion error utilized in [6] is logically incorrect as it will not satisfy the unit norm constraint of the unit quaternion (look at Section 6 for more details on this). The simulated results in [6] show some satisfactory results because the system is linearized and linear controls are utilized where these results are valid only in close neighborhood around an equilibrium point. Hence in our research, controls are designed for NL rotational equations of motion that provide global closed-loop stability of the system all the while achieving stringent pointing accuracy requirement posed on IRASSI's ACS.

NonLinear(NL) System and Control	Linear/Linearized System and Control
<ol style="list-style-type: none"> 1. NL model provides global attitude control (GAC), i.e., that handles large angle and angular velocity manoeuvres. 2. Suitable for arbitrary changes to spacecraft attitude. 3. Provides closed loop global Asymptotic Stability. 4. Robust towards initial conditions. 5. Represents actual system. 	<ol style="list-style-type: none"> 1. Linear/linearized model gives local attitude control (LAC), i.e. LAC handles relatively small attitude and angular velocity changes as they evolve close to neighbourhood of the equilibrium point. 2. LAC appropriate in presence of small disturbances. 3. Provides closed loop local Asymptotic stability. 4. Not robust towards initial conditions. 5. Does not represent actual system.

Table 3 Comparison of Nonlinear and Linear Control systems.

5. REFERENCE FRAMES REQUIRED FOR IRASSI SPACECRAFT ATTITUDE CONTROL

For the attitude control (and attitude estimation of IRASSI-satellite, as shown in [2], [3] and [4]) of the IRASSI satellites, an Earth-Centered Inertial (ECI) and body-fixed reference frame fixed to IRASSI-satellite are used. ECI is an inertial system with its origin at the center of mass (com) of the earth, with the coordinate axes z_I and x_I pointing to the North pole and the vernal equinox respectively. Axis y_I completes the right-handed coordinate system. The body-fixed reference frame of IRASSI is shown in Figure 1b, where X_{sc} points outward of the telescope boresight towards the celestial target, Z_{sc} points downward normal to the sunshield and Y_{sc} completes the right-handed coordinate system.

6. SPACECRAFT ROTATIONAL EQUATIONS OF MOTION

The work in this section is carried out within sub-work package 5.1. Rotational Equations of motion of a rigid spacecraft described in quaternion parameter includes its dynamics and kinematics equations as

shown in Eq. 2 and Eq. 1 respectively, where $\Omega(\omega) = \begin{bmatrix} 0 & \omega_3 & -\omega_2 & \omega_1 \\ -\omega_3 & 0 & \omega_1 & \omega_2 \\ \omega_2 & -\omega_1 & 0 & \omega_3 \\ -\omega_1 & -\omega_2 & -\omega_3 & 0 \end{bmatrix}$, $\Xi(q) = \begin{bmatrix} q_4 & -q_3 & q_2 \\ q_3 & q_4 & -q_1 \\ -q_2 & q_1 & q_4 \\ -q_1 & -q_2 & -q_3 \end{bmatrix}$ and $\omega \times = \begin{bmatrix} 0 & -\omega_3 & \omega_2 \\ \omega_3 & 0 & -\omega_1 \\ -\omega_2 & \omega_1 & 0 \end{bmatrix}$ is the skew-symmetric cross-product matrix. Equation

3 describes the unit norm constraint of the unit quaternion which should always be maintained [5].

Equations 4 and 5 describe the multiplicative quaternion error and additive angular velocity error formulation required for spacecraft attitude control development as shown in later sections, where ω_d and q_d are the desired angular velocity and desired quaternion respectively.

$$\dot{q} = \frac{1}{2}\Omega(\omega)q = \frac{1}{2}\Xi(q)\omega \quad (1)$$

$$\dot{\omega} = J^{-1}(-[\omega \times]J\omega + u + u_d) \quad (2)$$

$$||q||^2 = 1 \quad (3)$$

$$q_e = q \otimes q_d^{-1} \quad (4)$$

$$\omega_e = \omega - \omega_d \quad (5)$$

The external disturbance torque u_d considered for IRASSI spacecraft attitude control formulation includes three disturbance torques acting on the spacecraft, i.e. gravity-gradient torque (GG), solar radiation pressure (SRP) torque and a third constant torque for unforeseen disturbances (see Section 7). Reference [6] modifies the standard spacecraft kinematic equation Eq. 1 to include small constant orbital velocity of

IRASSI spacecraft $n_0 = \sqrt{\frac{\mu_1 + \mu_2}{r_0}}$ in it but does not modify the standard spacecraft dynamic equation Eq. 2

for the same. Hence, the control analysis carried out in [6] is inconsistent and unreliable. For our work, we use standard spacecraft kinematic and dynamic equations for designing control input torques u because the numerical value of n_0 is of the order of 10^{-10} which is ≈ 0 , hence our control analysis presented in this document is consistent and correct. r_0 in n_0 formula is the position of the spacecraft's center of mass relative to the Sun-Earth/Moon barycenter (see Figure 8) and, μ_1 and μ_2 are the gravitational constants of the two primaries (please look at Section 7 and [7]). And even though the final kinematic equation in [6] is correct, there is one significant error in its derivation where the 'application of transport theorem' in Eq. 3.74 is incorrect as it is missing minus sign on both sides of equation. Finally, since this year-long short research study is focused on the feasible attitude control algorithms that can achieve IRASSI's high pointing accuracy, our work is focused on the control algorithms and not the orbital motion of IRASSI satellites, which is out of scope of this study due to time-restriction.

The rotation parameter employed for spacecraft rotational equations of motion description are unit quaternions because of its obvious advantages as follows (refer to [5] and [8] for detailed description of quaternions and its algebra).

Advantages:

- I. They provide a compact attitude representation (with only 1 redundant parameter) that avoids any singularities for rotations between $0^\circ - 360^\circ$,
- II. Rotational kinematics in terms of quaternions are bilinear,
- III. The algebraic attitude matrix in terms of quaternions avoids transcendental functions and
- IV. They require simple successive rotations operation analogous to successive matrix rotations.

But, with all these advantages comes two disadvantages which are as follows.

Disadvantages:

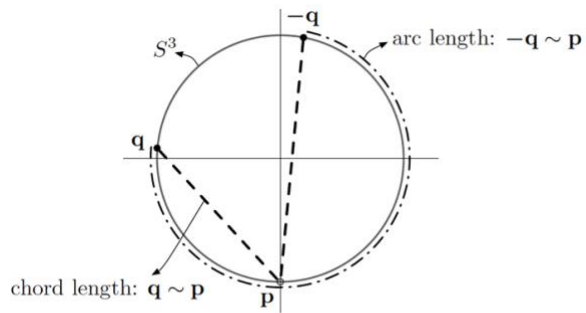
- I. **Maintenance of Quaternion Unit norm constraint:** Firstly, error quaternion shouldn't be computed as additive error as this leads to unit norm constraint violation.
- II. **Unwinding Problem in developing continuous controls with Quaternions:** Secondly, unit quaternions inherently possess a sign ambiguity because it doubly covers the *Special Orthogonal* $SO(3)$ space. In continuous feedback control, this property combined with the existence of an extra unstable equilibrium (shown in Figure 6 [9]) of quaternion leads to the *unwinding phenomenon* (demonstrated in Figure 7 [9]). This causes the spacecraft to traverse a longer geodesic as opposed to a shorter geodesic rotation. This problem is resolved by employing signum function $\text{sign}(q_{e4})$ in controls appropriately which takes into account the sign of the scalar quaternion component, where for a scalar number x

$$\text{sign}(x) = \begin{cases} -1, & \text{if } x < 0 \\ 0, & \text{if } x = 0 \\ 1, & \text{if } x > 0 \end{cases} \quad (6)$$

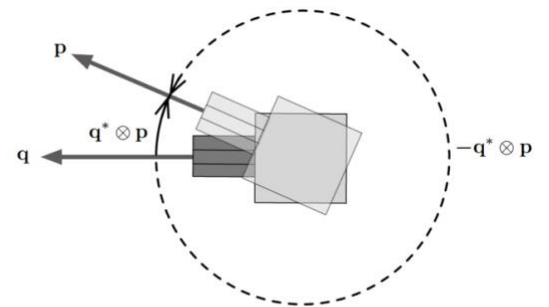
Representations	Stable Equilibrium	Unstable Equilibria
Rotation Matrix $SO(3) \times \mathbb{R}^3$	$\begin{bmatrix} 1 & 0 & 0 \\ 0 & 1 & 0 \\ 0 & 0 & 1 \end{bmatrix}$	$\begin{bmatrix} 1 & 0 & 0 \\ 0 & -1 & 0 \\ 0 & 0 & -1 \end{bmatrix}, \begin{bmatrix} -1 & 0 & 0 \\ 0 & -1 & 0 \\ 0 & 0 & 1 \end{bmatrix}, \begin{bmatrix} -1 & 0 & 0 \\ 0 & 1 & 0 \\ 0 & 0 & -1 \end{bmatrix}$
Unit quaternion $S^3 \times \mathbb{R}^3$	$\begin{bmatrix} 0 \\ 0 \\ 0 \\ 1 \end{bmatrix}$	$\begin{bmatrix} 0 \\ 0 \\ 0 \\ -1 \end{bmatrix}$

Figure 6 Stable and Unstable equilibria corresponding to the continuous feedback control law using the rotation matrix and unit quaternion. Extracted from [9].

Since q and $-q$ are on the opposite hemisphere of S^3 , we limit q to hemisphere in which $q_4 \geq 0$, which leads to θ being limited to $[-\pi, \pi]$, which in turn leads to discontinuous control law. Hence, this also prevents Global Asymptotic Stability (GAS) in sense of Lyapunov leading to a relaxed "almost" GAS where asymptotic stability is defined over an "open" and dense set in $SO(3)$. This means that these control algorithms provide local Asymptotic Stability in the sense of Lyapunov as shown in Section 11.



Chord length used to determine which arclength is shorter.
 $\|p - q\|$ shorter than $\|p + q\|$.



Attitude error of p w.r.t. to q and $-q$.

Figure 7 Unwinding Phenomenon depiction. Figure extracted from [9].

7. IRASSI SPACECRAFT EXTERNAL DISTURBANCES

The work in this section is carried out within work package 5.1. Total external disturbance torque u_d as shown in Eq. 2 of spacecraft dynamics euler-equation comprises of two external disturbance torques acting on the IRASSI spacecraft, i.e. gravity-gradient torque u_{gg} and a constant external torque u_{const} which is a combination of solar radiation pressure (SRP) and other unforeseen disturbances acting on the spacecraft explained below.

$$u_d = u_{gg}^b + u_{const} \quad (7)$$

7.1. Gravity-Gradient Torque

Gravity gradient torque exerted by two primaries Sun and Earth/Moon system acting IRASSI spacecraft orbiting Sun-Earth/Moon Lagrange point 2, solved as a restricted three-body problem extracted from [7] is given by Eq. 8 as shown in Figure 8,

$$u_{gg}^o = -3 \left(\frac{\mu_1}{r_1^3} + \frac{\mu_2}{r_2^3} \right) \hat{\mathbf{R}} \times \mathbf{J} \hat{\mathbf{R}} \quad (8)$$

where $\mu_1 = GM_1, \mu_2 = GM_2$ are the gravitation parameters of the two primaries, i.e. Sun and Earth/Moon system respectively, r_1 and r_2 are the positions of these primaries from the center of mass of the orbiting spacecraft respectively, \mathbf{J} is the spacecraft inertia tensor, \mathbf{R} is the distance between the Sun-Earth/Moon system barycenter and spacecraft center of mass. Since the spacecraft is fixed to Lagrange point 2, it will orbit the barycenter of this system in a circular orbit together with the primaries moving in a constant angular velocity [7]. Transforming u_{gg}^o from orbital frame to spacecraft body frame using the matrix $\mathbf{A}(\mathbf{q})$ from [5] is given by Eq. 12. This transformation is explained as follows.

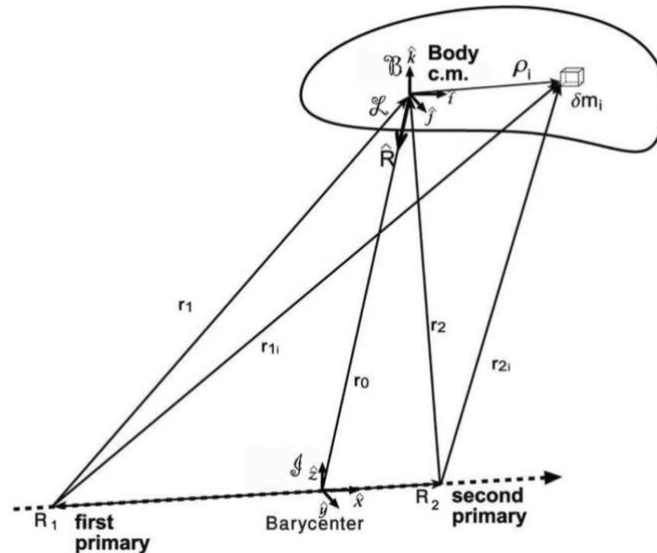


Figure 8 Gravity-gradient torque on rigid spacecraft in restricted three-body problem. Extracted from [7].

Consider a general attitude transformation matrix from orbital frame to the body frame

$$\vec{B} = \mathbf{A}^{B/O} \vec{L} \quad (9)$$

where $\vec{B} = [\hat{B}_1 \ \hat{B}_2 \ \hat{B}_3]$ is the body frame vector and $\vec{\mathcal{L}} = [\hat{\mathcal{L}}_1 \ \hat{\mathcal{L}}_2 \ \hat{\mathcal{L}}_3]$ is the orbital frame vector. And,

$$A^{B/\mathcal{L}} = \begin{bmatrix} A_{11} & A_{12} & A_{13} \\ A_{21} & A_{22} & A_{23} \\ A_{31} & A_{32} & A_{33} \end{bmatrix} \quad (10)$$

The components of R are the components of $\hat{\mathcal{L}}_3 = A_{13}\hat{B}_1 + A_{23}\hat{B}_2 + A_{33}\hat{B}_3$. Additionally,

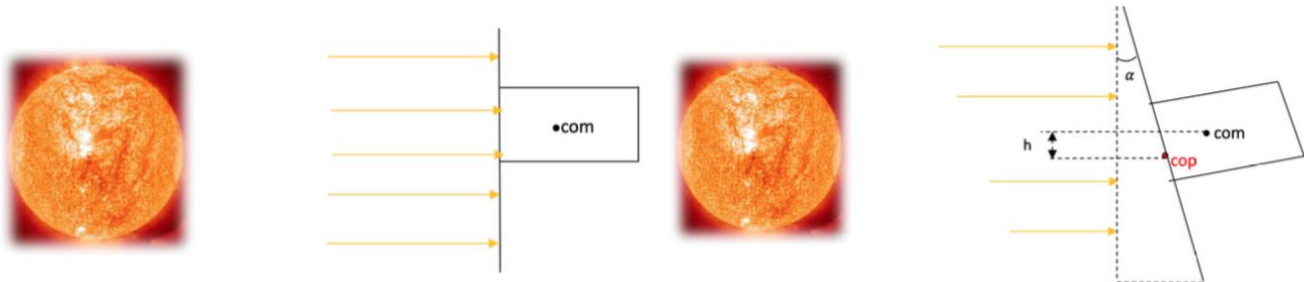
$$\hat{R} \times J\hat{R} = A_{23}A_{33}(J_3 - J_2) - A_{23}A_{33}(J_3 - J_2) + A_{23}A_{33}(J_3 - J_2) \quad (11)$$

Components of $A^{B/O}$ corresponding to matrix A(q) from [5] are substituted to get the final equation as

$$u_{gg}^b = -3 \left(\frac{\mu_1}{r_1^3} + \frac{\mu_2}{r_2^3} \right) \begin{bmatrix} 0 & -1 + 2(q_1^2 + q_2^2) & 2(q_2q_3 + q_1q_4) \\ 1 - 2(q_1^2 + q_2^2) & 0 & -2(q_1q_3 - q_2q_4) \\ -2(q_2q_3 + q_1q_4) & 2(q_1q_3 - q_2q_4) & 0 \end{bmatrix} J \begin{bmatrix} 2(q_1q_3 - q_2q_4) \\ 2(q_2q_3 + q_1q_4) \\ 1 - 2(q_1^2 + q_2^2) \end{bmatrix} \quad (12)$$

7.2. Constant External Torque

Another external disturbance torque considered in this problem is a constant torque $u_{\text{const}} = u_{\text{SRP}} + u_c$ which is a sum of the SRP torque acting on the spacecraft and any other unforeseen additional disturbances. The force due to SRP can be obtained from the author's paper titled "Attitude Determination and Control System Design of Sub-Arcsecond Pointing Spacecraft" with doi [10.2514/1.G005116](https://doi.org/10.2514/1.G005116). Two cases of SRP torques are explained in journal paper and as shown in Figure 9. Finally, for the simulations, we consider $u_{\text{const}} = 1.18 \times 10^{-3} \text{ N-m}$. For more details on SRP, please refer to [10].



(a) Solar Radiation Pressure perpendicular to the Spacecraft surface.

(b) Solar Radiation Pressure not perpendicular to the Spacecraft surface.

Figure 9 Solar Radiation Pressure cases.

8. SLIDING MODE CONTROL (SMC)

The work in this section is carried out within work package 5.1.

8.1. Methodology

SMC [11], [5] is a controller that steers the system trajectory to the properly chosen sliding manifold/surface (see Figure 10) and thereafter maintains the motion on the manifold by means of a control, thus exploiting the main features of the sliding mode: its insensitivity to external and internal disturbances matched by the control, ultimate accuracy, robustness to model uncertainties and finite-time convergence of the sliding variables to zero. It is a two-part controller, where first part involves designing a sliding surface such that the sliding motion satisfies design specifications. Second part is concerned with the selection of a control law that will make the sliding surface attractive to the system state. It is also a two-phase controller as shown in Figure 10, where, in first phase called as “reaching phase” the system trajectory is forced to move from an initial condition to the chosen sliding surface. And the second phase is called the “sliding phase” in which, once the sliding surface is reached, SMC keeps the states in the close neighborhood of the sliding surface for all future time for ‘real SMC’ and on the surface for ‘ideal SMC’ [12]. The state-feedback control law can switch from one continuous structure to another based on the current position in the state space. Hence, SMC is called a variable structure control method. But it exhibits a chattering phenomenon due to parasitic dynamics and switching time delay [12], which is perceived as oscillations about the sliding manifold which may excite higher frequencies of a spacecraft and may cause possible damages to the actuators. This is handled by smoothing the control input via variable thickness boundary layer method that computes the saturation function as a function of the sliding manifold and its boundary layer thickness. SMC is also the “BEST CONTROLLER” in modern control theory so far due to its property of achieving theoretically perfect accuracy where the state trajectories remain on the sliding surface in the “sliding phase”.

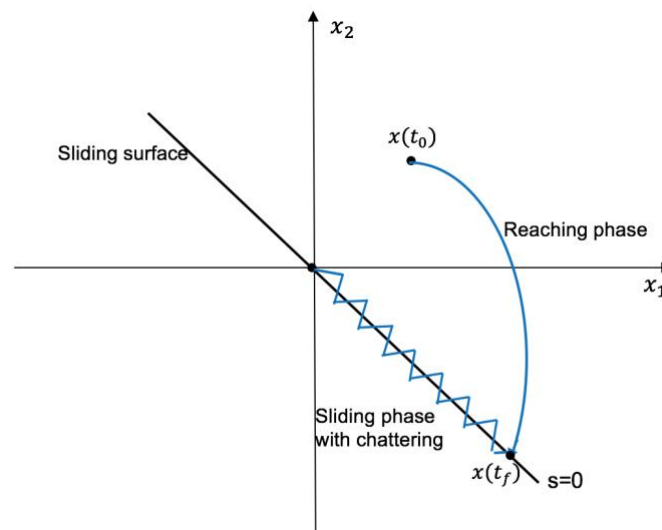


Figure 10 Sliding Mode Control depicting the sliding surface, chattering and two phases namely reaching and sliding phase.

For classical first-order SMC, the chosen sliding surface is $\sigma = \omega_e + \Lambda \text{sign}(q_{e4})q_{e1:3}$, where Λ is the sliding surface slope, where $\text{sign}(q_{e4})$ is used to eliminate the *unwinding phenomenon*, ω_e and $q_{e1:3}$ are the angular velocity error and quaternion error vectors as depicted in Eq. 4 and Eq. 5 respectively. Take notice that first time-derivative of σ introduces the control u in $\dot{\sigma}$. With Eq. 1 and Eq. 2 as the system, Eq.

12 as the gravity-gradient torque and $u_{\text{const}} = 1.18 \cdot 10^{-3} \text{ N-m}$ as the combination of SRP and constant external torque, the control for this system is given as [5]

$$u_{SMC} = J(-\Lambda \dot{q}_{e1:3} + \dot{\omega}_d) + [\omega \times]J\omega - JG\text{sat}(\sigma_i, \varepsilon_i) \quad (13)$$

where $i = 1, 2, 3$ and $\text{sat}(\sigma_i, \varepsilon_i)$ is the saturated function with arguments as the sliding surface σ and ε , where ε is the sliding surface boundary layer and G is a positive quantity. For more details, check [11] and [5]. There are different ways of deriving SMC. Reference [13] shows that it can be analytically formulated as an Optimal control problem and the sliding surface used above leads to an optimal performance. For more details, check the reference.

$$\text{sat}(\sigma_i, \varepsilon_i) = \begin{cases} -1, & \text{if } \sigma_i < -\varepsilon_i \\ \frac{|\sigma_i|}{\varepsilon_i}, & \text{if } |\sigma_i| \leq \varepsilon_i \\ 1, & \text{if } \sigma_i > \varepsilon_i \end{cases} \quad (14)$$

8.2. Simulation Results

This section illustrates the simulation results of SMC for large and small angle tracking rest-to-rest (regulation) maneuvers. The moment of inertia matrix for an IRASSI spacecraft is its principal moment of

inertia $J = \begin{bmatrix} 2059.5 & 0 & 0 \\ 0 & 5954.2 & 0 \\ 0 & 0 & 5974.3 \end{bmatrix} \text{ kg} - \text{m}^2$. An accuracy of $\leq 0.3 \text{ arcsec}$ is required from all the controllers. The two cases for which the results are demonstrated are:

- Large Angle Maneuver: $\theta_0 = [14 \quad 14 \quad 14]^\circ$ and $\theta_d = [30 \quad -20 \quad 1]^\circ$.
- Small Angle Maneuver: $\theta_0 = [14 \quad 14 \quad 14]^\circ$ and $\theta_d = [13 \quad 13 \quad 13]^\circ$.

The initial and final angular velocities are $\omega_0 = [0, 0, 0]$ and $\omega_d = [0, 0, 0]$ because it is the regulation case, i.e. rest-to-rest maneuvers. The simulation time is 500 seconds with 1 second as the step-size of the integration. These initial conditions are the same for PD controller simulation in Section 10 and LQR controller simulation in Section 9. The high accuracy pointing (Table 1) that IRASSI imposes on “Attitude determination/estimation and control system(ADCS, Figure 4)” is for “small angle maneuvers” because once the science observations start, i.e. once the spacecraft points to a scientific target, there might be only small deviations in the spacecraft attitude from this scientific target. But since “large angle maneuvers” are required by many other telescopic and non-telescopic space missions and because these are the most difficult maneuvers to perform due to nonlinearities of the system dynamics, properties of attitude parameters utilized, accumulation of disturbances and exposure to varying disturbances, we check the feasibility of the control algorithms analyzed in this document in achieving tens-of-subarcsec accuracy for these maneuvers too. So, this is the extra work done within IRASSI 2 phase 1 project. Every extra work in this project is extra because it was not proposed in the technical proposal and hence no financial aid was received to perform this work.

The tuning parameters in SMC are $G, \Lambda = 1$ and ε_i with $i=1,2,3$. These parameters are tuned by trial and error. One can tune them using an adaptive algorithm but this was out of scope of this project due to short time. Figure 11-Figure 13 and Figure 14-Figure 16 shows the results for large angle maneuver cases 1 and 2

respectively, where the tuning parameters G and ε_i in both cases are different. In case 1 the maximum control input torques calculated are very high, i.e. nearly $[40, 320, 210]$ N-m in three axes of the spacecraft as shown in Figure 12b which is due to the fact that the quaternion errors for this case are $[0.05, 0.02, 0.02]$ arcsec in the three-axes as shown in Figure 12a. Comparing these values to the maximum control torques and quaternion errors for large angle case 2, as shown in Figure 15b and Figure 15a are $[-21, -48, 32]$ N-m and $[0.1, 0.12, 2.9]$ arcsec respectively in three axes. The maximum control torques are one order higher in case 1 as compared to case 2 which is due to the fact that the regulation pointing accuracies are approximately an order better in this case. Hence, better the accuracies, more control input torques are required to achieve it which is in line with our common sense. Hence, caution is advised for IRASSI 2 Phase 2 where the actuators need to be selected to provide these control torques.

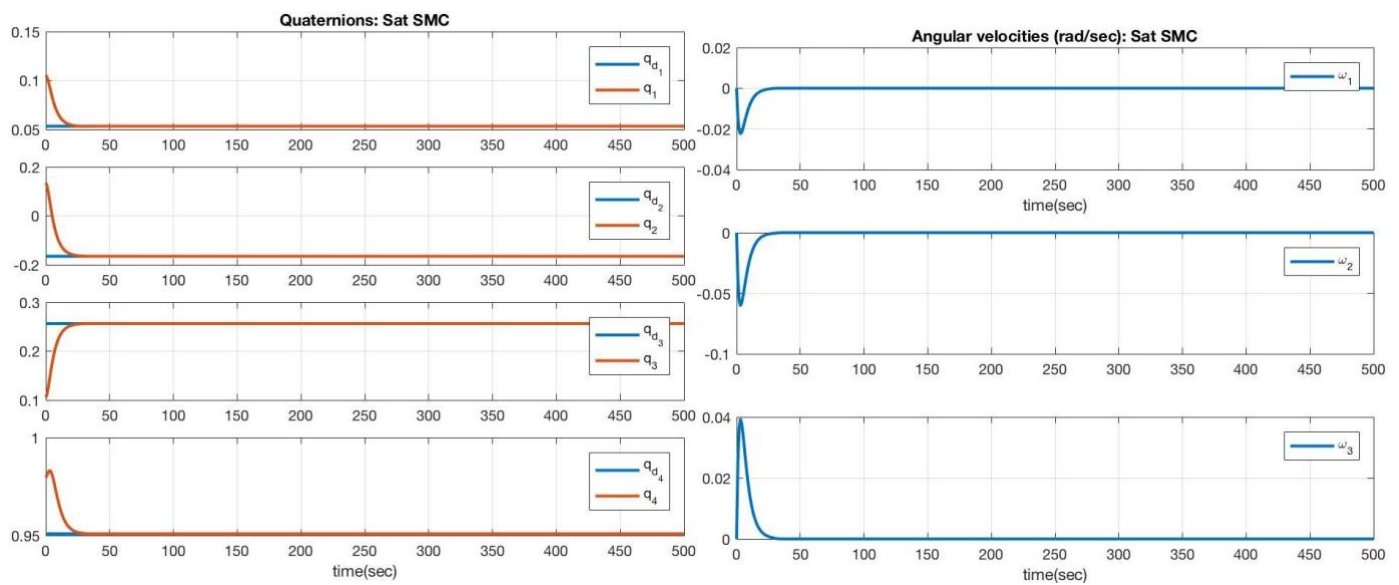


Figure 11 Large Angle Slew case 1: a. Quaternion Tracking b. Angular velocity Tracking.

Figure 11a and b show the quaternion tracking and angular velocity tracking for large angle maneuver case 1 which is very accurate. Analogously, for large angle case2 Figure 14a and b demonstrate accurate quaternion and angular velocity tracking. Figure 13a and Figure 16a illustrate that the sliding surface goes to zero which is in accordance to the invariant sliding condition of SMC. Phase plane plots in Figure 13b and Figure 16b demonstrate that the state trajectories go to zero, i.e. to zero sliding surface in accordance to the SMC derivation.

Figure 17-Figure 19 illustrate the results for small angle maneuvers where an accuracy of $[0.05, 0.02, 0.02]$ arcsec with maximum control torques of $[-3, -13, -8]$ N-m is achieved in three-axes respectively as shown in Figure 18a and Figure 18b. Figure 17a and b show an accurate quaternion and angular velocity tracking in small angle reorientation case. Table 4 lists the accuracies achieved and the corresponding maximum control input torques calculated to achieve these accuracies for the three simulated cases of SMC. It shows that in order to get higher accuracies for large angle slews, higher control torques are required. But for small angle maneuvers, small control torques are required for high pointing accuracies.

Table 8 compares the approximate maximum control torques calculated by all the five controllers namely SMC, LQR, Linear PD, Negative NL PD and Positive NL PD to obtain accuracy ≤ 0.1 arcsec. It thus validates

the title of SMC as the highly accurate „best controller in modern control theory“ because it applies the least amount of control torques to obtain the accuracies ≤ 0.1 arcsec.

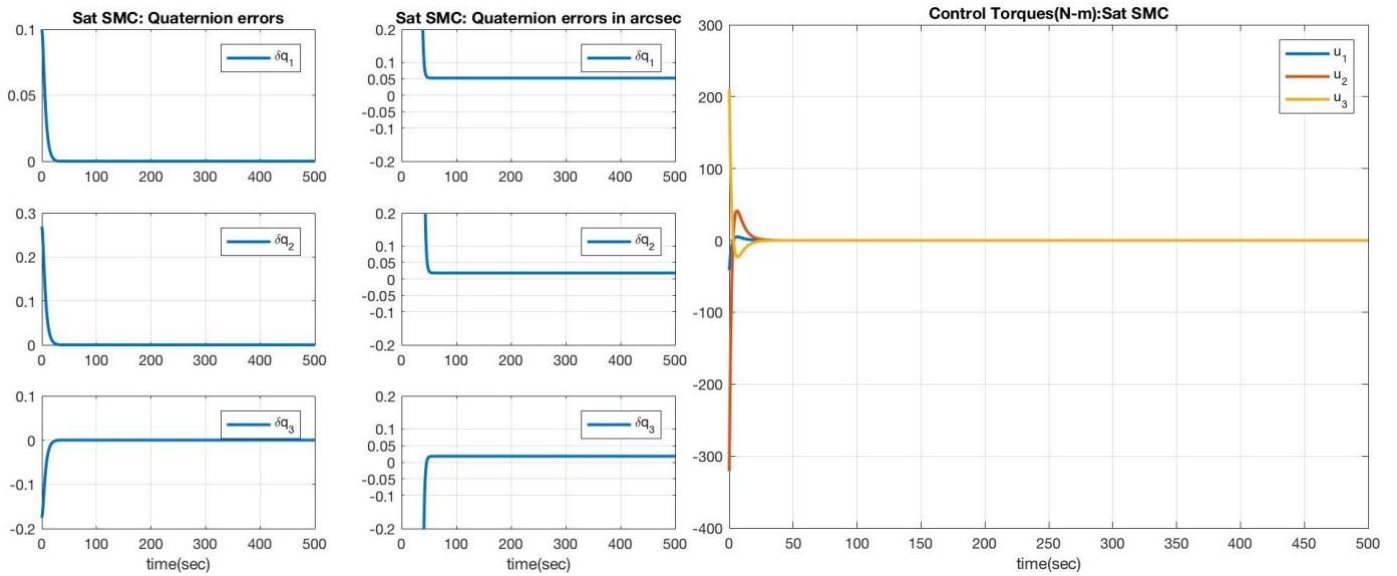


Figure 12 Large Angle Slew case 1: a. Quaternion Errors b. Control Torques.

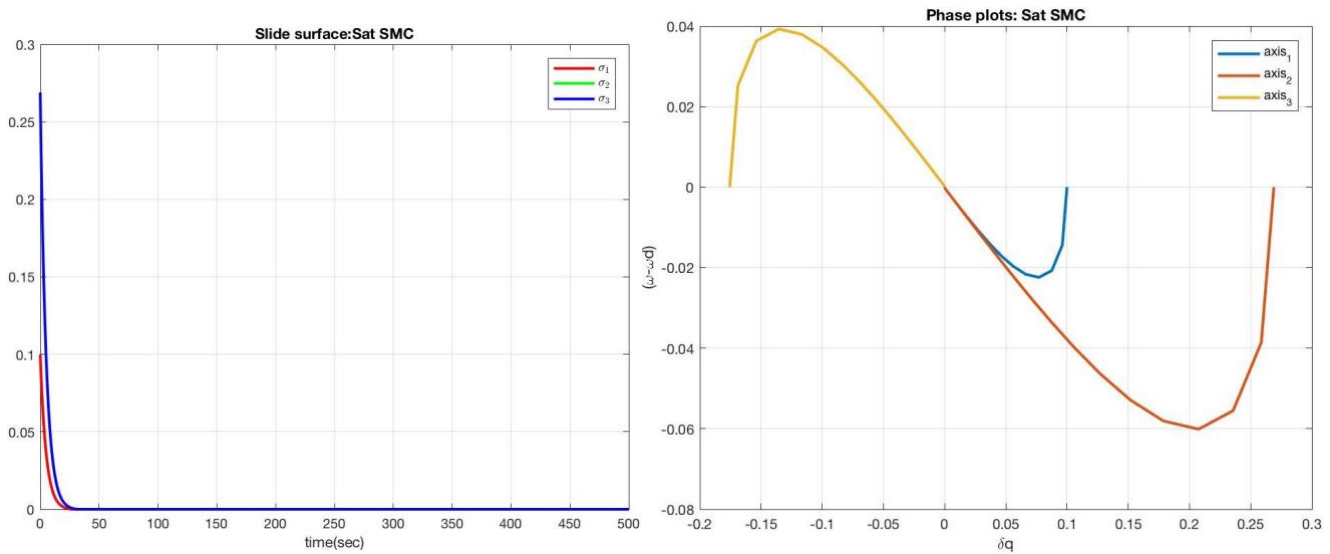


Figure 13 Large Angle Slew case 1: a. Sliding Surface b. Phase Plots.

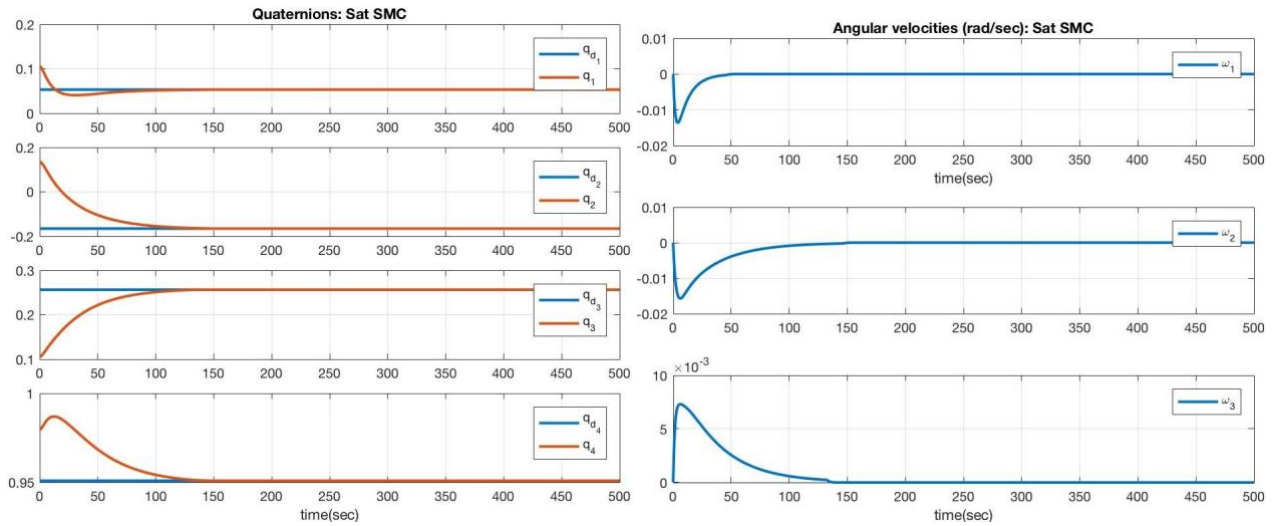


Figure 14 Large Angle Slew case 2: a. Quaternion Tracking b. Angular velocity Tracking.

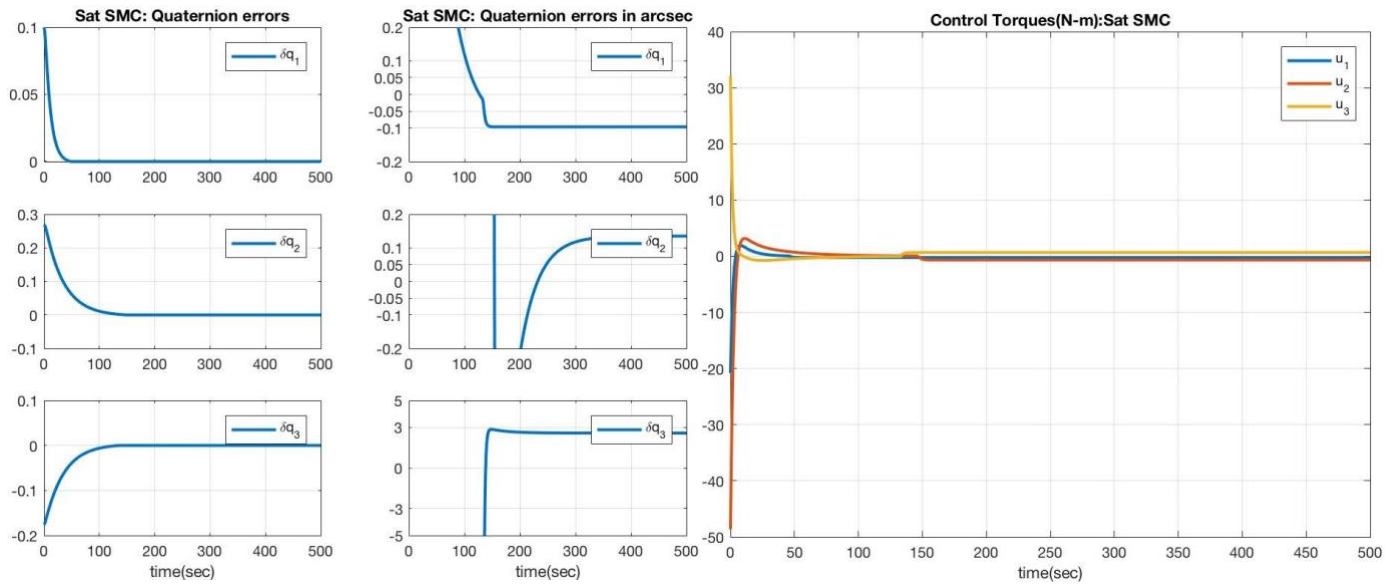


Figure 15 Large Angle Slew case 2: a. Quaternion Errors b. Control Torques.

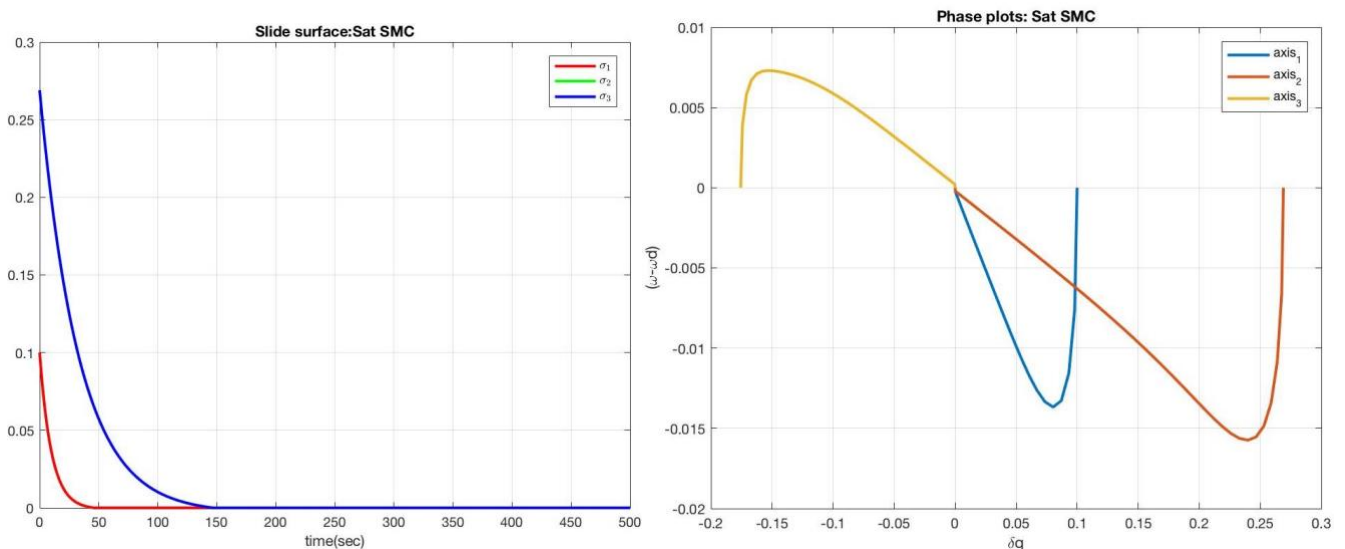
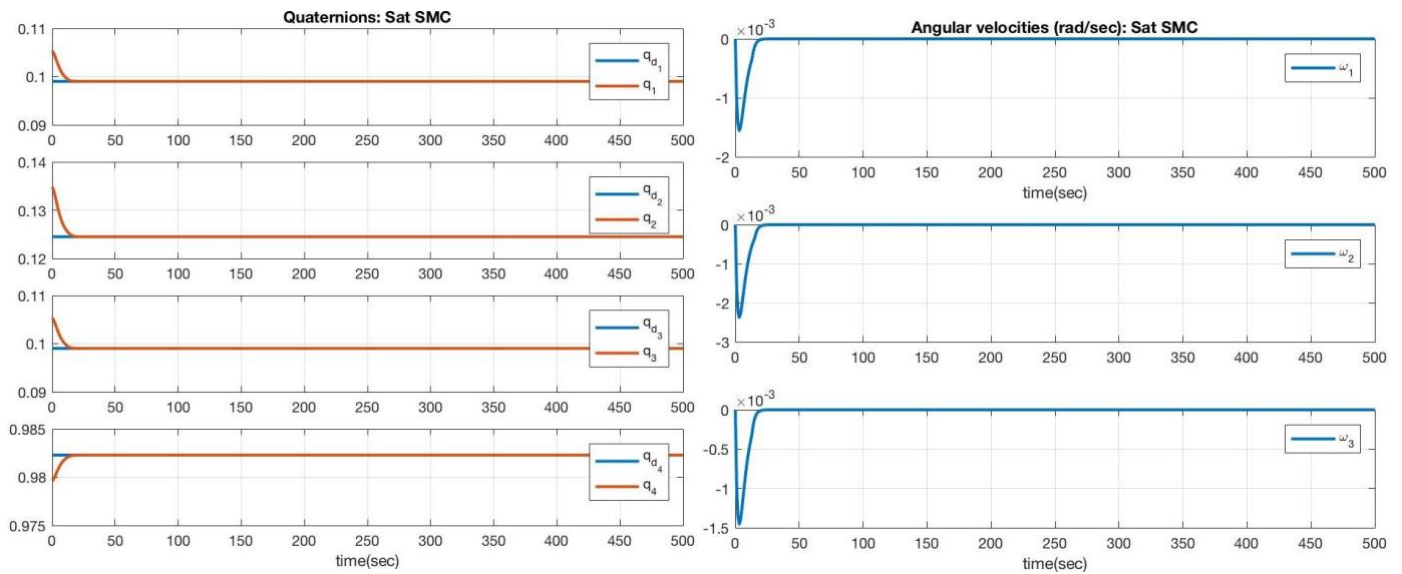
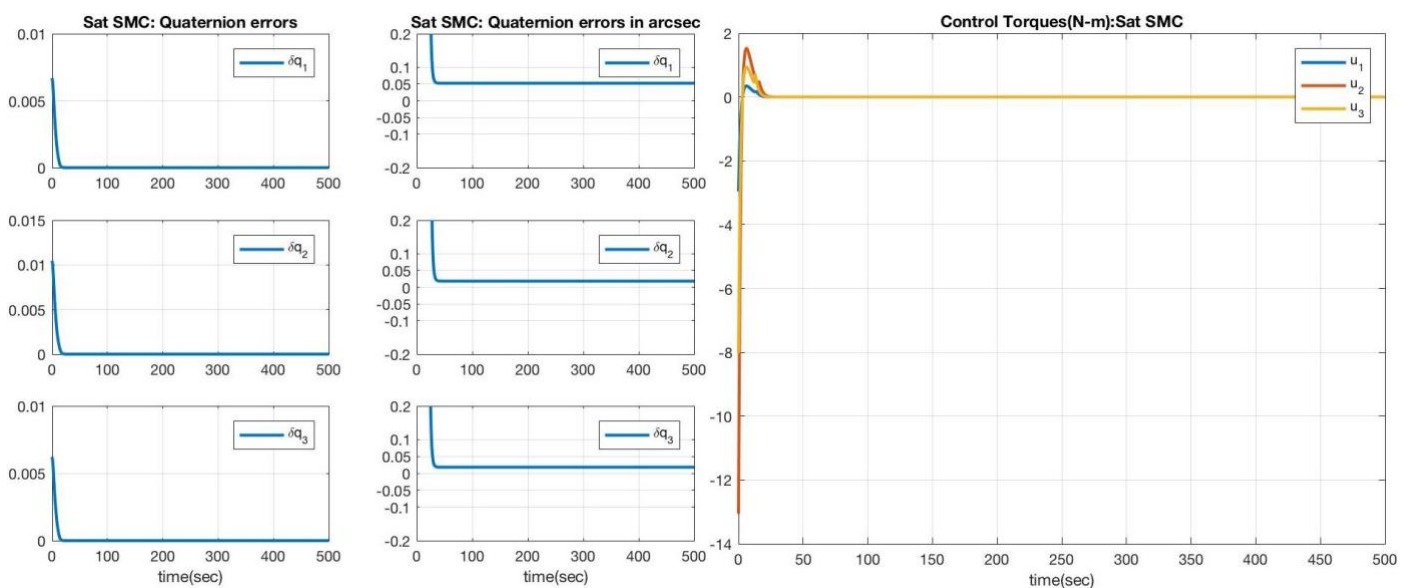


Figure 16 Large Angle Slew case 2: a. Sliding Surface b. Phase Plots.

SMC Cases	Accuracy Achieved (arcsec)	Max. Control torque (N-m)
Large angle slew case 1	[0.05, 0.02,0.02]	[40, 320,210]
Large angle slew case 2	[0.1, 0.12, 2.9]	[-21, -48, 32]
Small angle slew	[0.05, 0.02,0.02]	[-3,-13,-8]

Table 4 Accuracies Achieved by SMC Cases.**Figure 17 Small Angle Slew: a. Quaternion Tracking b. Angular velocity Tracking.****Figure 18 Small Angle Slew: a. Quaternion Errors b. Control Torques.**

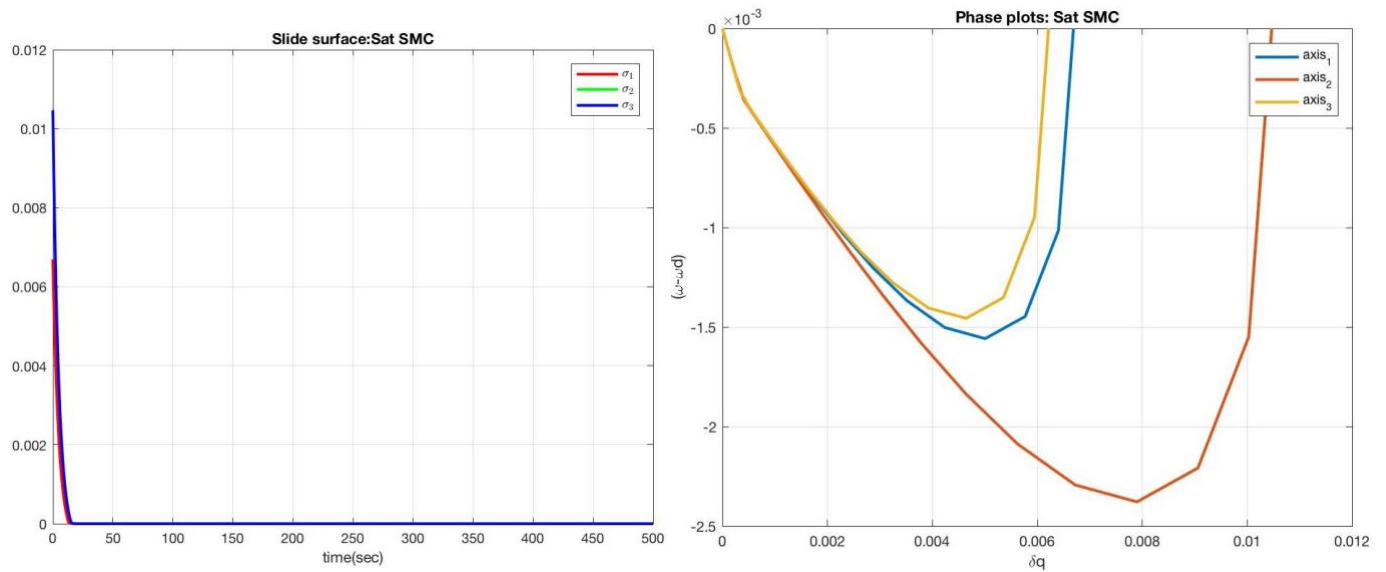


Figure 19 Small Angle Slew: a. Sliding Surface b. Phase Plots.

9. LINEAR QUADRATIC REGULATOR (LQR)

The work in this section is carried out within sub-work package 5.1.

9.1. Methodology

Linear Quadratic Regulator is an Infinite Horizon optimal controller, i.e. it is formulated using optimal control methodology. This problem has quadratic cost functional J as a quadratic in state and control, where Q_1 and R are their respective cost/gain matrices.

$$J = \frac{1}{2} \int_0^{\infty} (x^T Q_1 x + u^T R u) dt \quad (15)$$

with linear/linearized dynamical system equation as

$$\dot{x} = Ax + Bu, \quad (16)$$

where A and B are constant state and input matrices and the state initial constraint is $x(0) = x_0$.

The assumptions that are made to solve this optimal control problem are

- Pair (A, B) is controllable leading to roots of Eq. 18 being in left-half plane,
- Pair (A, Q_1) is observable leading to every state 'showing up in/being associated with' the cost J ,
- Cost matrix $Q_1 \geq 0$, i.e. Q_1 is positive semidefinite leading to $(x^T Q_1 x)$ being positive definite. And $Q_1^T = Q_1$, i.e. Q_1 is symmetric matrix.
- Cost matrix $R > 0$, i.e. R is positive definite leading to R being invertible. And $R^T = R$, i.e. R is symmetric matrix.

Now form the Hamiltonian H [14] as follows where L is the lagrange term and λ is the lagrange multiplier.

$$H = L + \lambda^T \dot{x} = \frac{1}{2} (x^T Q_1 x + u^T R u) + \lambda^T (Ax + Bu) \quad (17)$$

Solve for costate equation and strong form of Pontryagin's principle equation as in Eq. 20. Optimal control has to lie on interior of the set u , but the interior of the set is from $-\infty$ to ∞ (i.e. there is no bounds on control).

$$\begin{aligned} \dot{\lambda} &= - \left[\frac{\partial H}{\partial x} \right]^T = -Q_1 x - A^T \lambda \\ \frac{\partial H}{\partial u} &= u^T R + \lambda^T B = 0 \end{aligned} \quad (18)$$

This gives the stable feedback controller as Eq. 21 with feedback matrix as $K = R^{-1} B^T S$ where positive matrix S is obtained by the Algebraic Riccati Equation (ARE) given by Eq. 22 and the optimal state solution is given by Eq. 23.

$$u_{LQR}^* = -R^{-1} B^T S x^* \quad (19)$$

$$-SA - A^T S + SBR^{-1}B^T S - Q = 0 \quad (20)$$

$$\dot{x}^* = (A - BR^{-1}B^T S)x^* \quad (21)$$

LQR feedback Eq. 21 guarantees the stability of the linearized closed loop system Eq. 18 and minimizes the cost function Eq. 17 which is a combined cost of cumulative control energy and system error. This analytical derivation of LQR guarantees its stability as follows.

- Eigenvalues of $(A - BR^{-1}B^T S)$ is in the open Left-half plane leading to x goes to 0. $x \rightarrow 0$ is also ensured by $S > 0$.
- LQR globally stabilizes NL system of equations [15].

- LQR is suboptimal since it is derived using linear/linearized equation of motion [15].

For the application of LQR to spacecraft attitude control, Eq. 1 and 2 have to be linearized according to Eq. 18 but a full quaternion-based linearized model of spacecraft equations of motion is not fully controllable [15], which is a main requirement for using LQR. Hence a reduced quaternion model using only quaternion vector components is utilized which is fully controllable as shown in Eq. 24 [15].

$$\begin{bmatrix} \dot{q}_1 \\ \dot{q}_2 \\ \dot{q}_3 \end{bmatrix} = \frac{1}{2} \begin{bmatrix} \sqrt{1 - q_1^2 - q_2^2 - q_3^2} & -q_3 & q_2 \\ q_3 & \sqrt{1 - q_1^2 - q_2^2 - q_3^2} & -q_1 \\ -q_2 & q_1 & \sqrt{1 - q_1^2 - q_2^2 - q_3^2} \end{bmatrix} \begin{bmatrix} \omega_1 \\ \omega_2 \\ \omega_3 \end{bmatrix} \quad (22)$$

Further, for quaternion tracking LQR, a multiplicative quaternion error dynamics [16] as shown in Eq. 25 [5] is utilized along with Eq. 2 which are linearized (Eq. 26) by using first order Taylor series expansion around the stationary point $\omega = 0, q_{1:3} = 0$ which are used to calculate the feedback gain matrix given in Eq. 21.

$$\delta \dot{q}_{1:3} = \frac{1}{2} [\delta q_{1:3} \times] \omega + \frac{1}{2} \delta q_4 \omega \quad (23)$$

$$\begin{bmatrix} \delta \dot{q} \\ \dot{\omega} \end{bmatrix} = \frac{1}{2} \begin{bmatrix} 0_{3 \times 3} & \frac{1}{2} I_{3 \times 3} \\ 0_{3 \times 3} & 0_{3 \times 3} \end{bmatrix} \begin{bmatrix} q \\ \omega \end{bmatrix} + \begin{bmatrix} 0_{3 \times 3} \\ J^{-1} \end{bmatrix} u = Ax + Bu \quad (24)$$

9.2. Simulation Results

LQR is simulated with Eq. 25 and Eq. 2 as the system, Eq. 12 as the gravity-gradient torque and $u_{\text{const}} = 1.18 \times 10^{-3} \text{N-m}$ as the combination of SRP and constant external torque for large and small angles tracking rest-to-rest (regulation) maneuvers. The controller design Eq. 21 utilizes Eq. 26 for calculating A and B matrices required for solving the ARE along with Q and R which are the tunable parameters as shown in Eq. 22.

Figure 20 and Figure 21 demonstrate the results of matlab simulation for two cases of large angle slew where cases 1 and 2 have different Q and R values. For case 1, $Q = 200I_{6 \times 6}$ and $R = 0.001I_{3 \times 3}$. Figure 20a illustrates the accurate quaternion and angular velocity tracking. Figure 20b shows that the pointing accuracy fluctuates between 0.4-0.6 arcsec obtained by applying reasonable control torques. In order to improve the pointing accuracies ≤ 0.1 arcsec, control torques were increased by increasing Q and decreasing R (which is case 2) to obtain an accuracy ≤ 0.1 arcsec as shown in Figure 21b at the cost of very high control input torques. Figure 21a demonstrates the perfect quaternion and angular velocity tracking for this case.

Analogous results were obtained for small angle rest-to-rest maneuvers as depicted in Figure 22 and Figure 23. Table 5 lists the pointing accuracies achieved by LQR for the two simulated cases, i.e. large and small angle slews. It is worth mentioning that a constant control effort is required when using LQR controller unlike SMC or PD controllers.

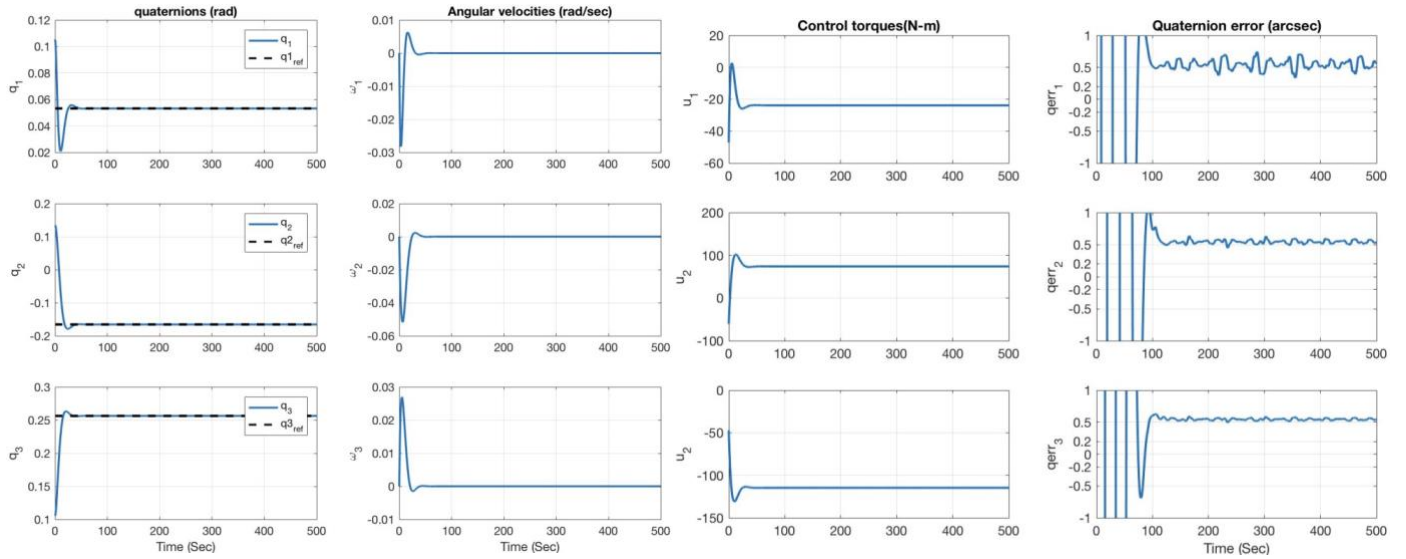


Figure 20 LQR Large Angle Manuever Case 1 a. Quaternion and Angular Velocity Tracking b. Control Torques and Quaternion errors.

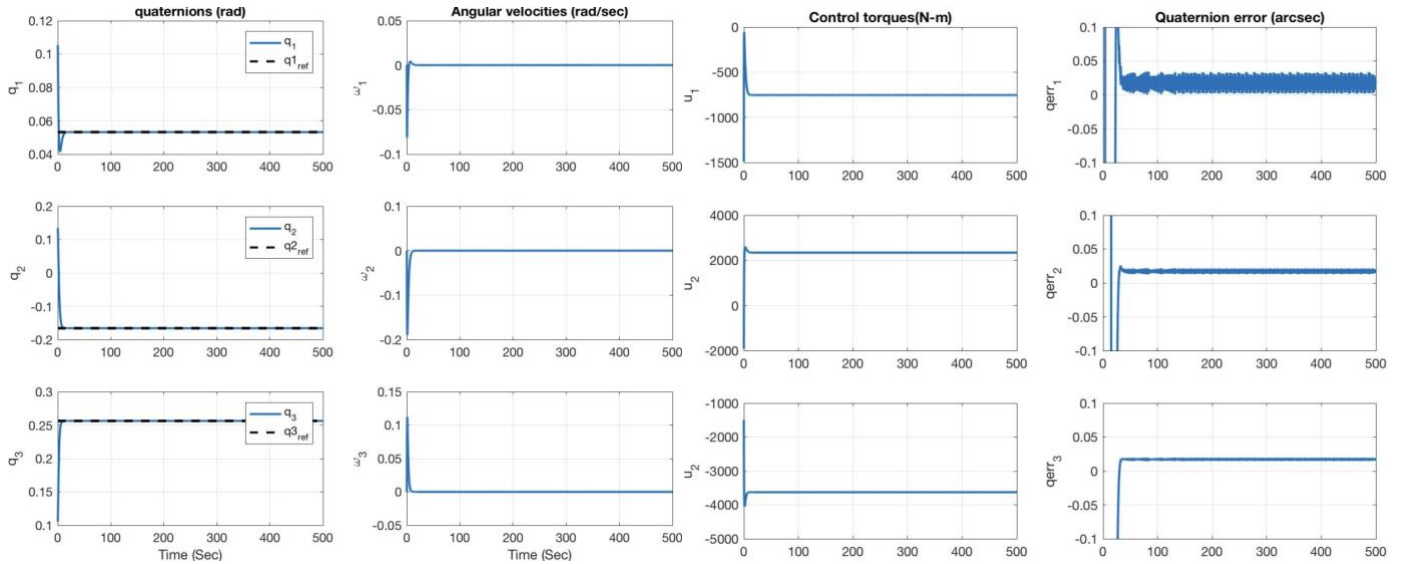


Figure 21 LQR Large Angle Manuever Case 2 a. Quaternion and Angular Velocity Tracking b. Control Torques and Quaternion errors.

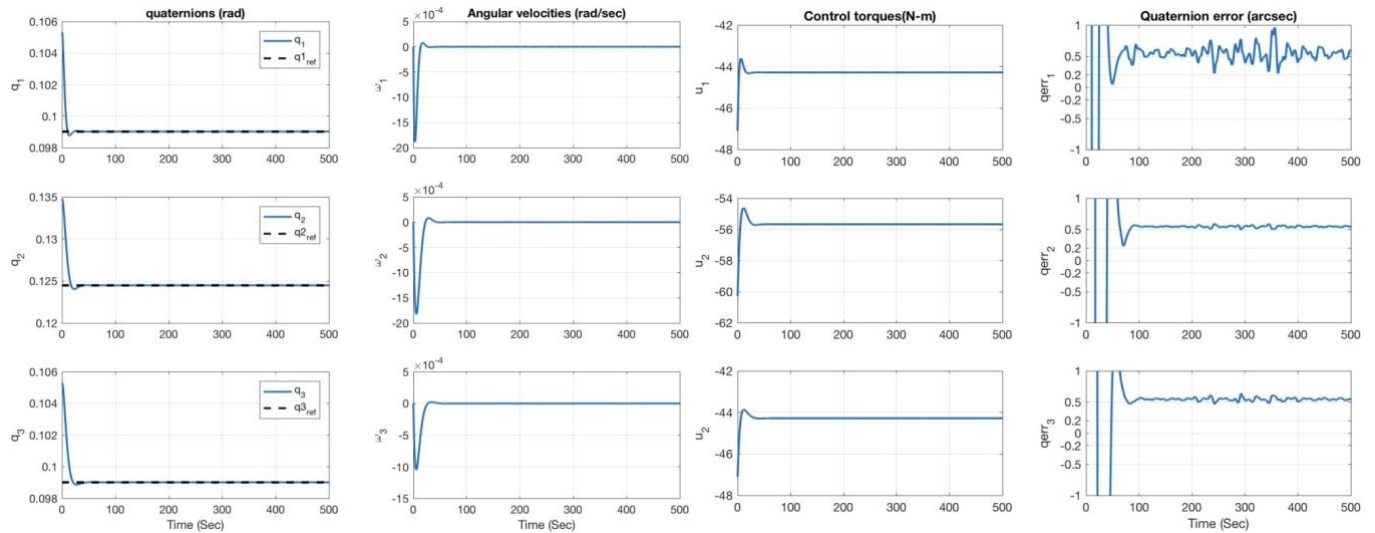


Figure 22 LQR Small Angle Manuever Case 1 a. Quaternion and Angular Velocity Tracking b. Control Torques and Quaternion errors.

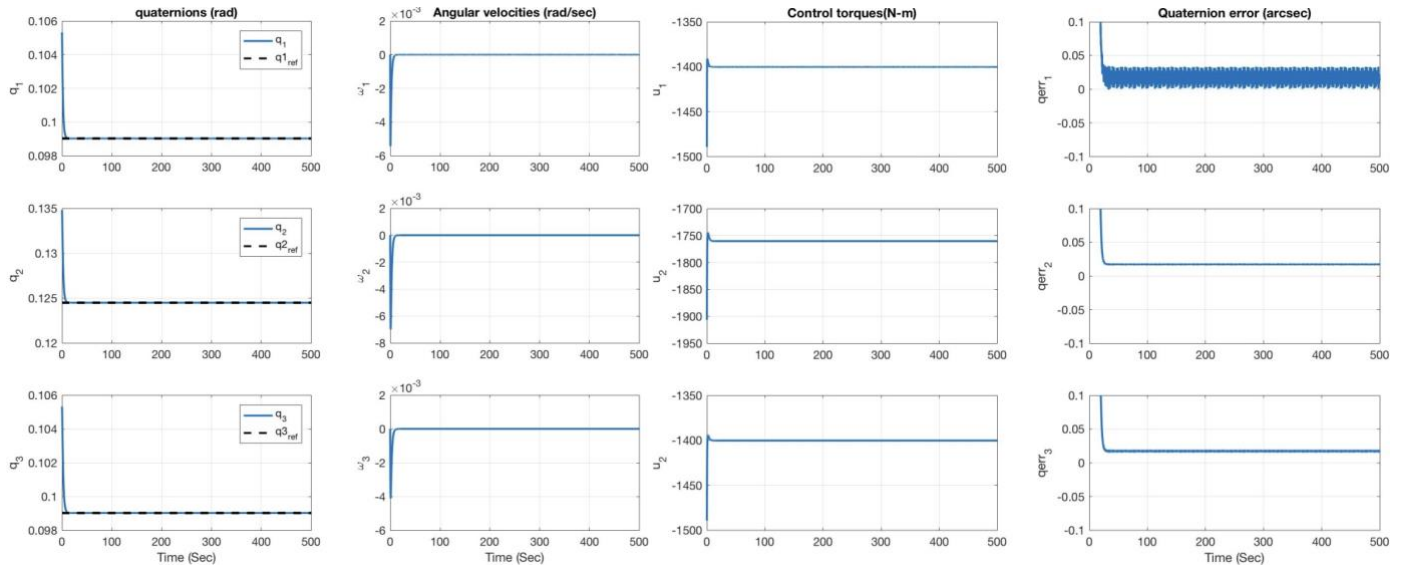


Figure 23 LQR Small Angle Manuever Case 2 a. Quaternion and Angular Velocity Tracking b. Control Torques and Quaternion errors.

LQR Cases	Accuracy Achieved (arcsec)	Maximum Control torque (N-m)
Large angle slew case 1	0.4-0.6 arcsec	[-48, 100,-120]
Large angle slew case 2	0.01-0.03 arcsec	[-1500, 2800,-4000]
Small angle slew case 1	0.4-0.6 arcsec	[-47, -61,-47]
Small angle slew case 2	0.01-0.03 arcsec	[-1400, -1760,-1400]

Table 5 Accuracies Achieved by LQR Cases.

10. LINEAR AND NONLINEAR PROPORTIONAL-DERIVATIVE (PD) CONTROL

The work in this section is extra work as this algorithm was not proposed in IRASSI2 phase 1 proposal.

10.1. Methodology

First PD controller that is investigated is a linear PD controller [5] and two other PD controllers that are investigated are NL PD controllers as given in Eq. 27 and Eq. 28 respectively.

$$u_{PD1} = -k_p \text{sign}(q_{e4})q_{e1:3} - k_d \omega \quad (25)$$

$$u_{PD2-3} = -k_p \text{sign}(q_{e4})q_{e1:3} - k_d (1 \pm q_{e1:3}^T q_{e1:3}) \omega \quad (26)$$

where a multiplicative quaternion error is utilized as described in Eq. 4. Signum of the scalar component of the quaternion is utilized appropriately in τ_{PD1} and τ_{PD2-3} to overcome unwinding phenomenon as explained in Section 6. The proportional and derivative gains k_p and k_d respectively are chosen by trial and error method to achieve the required pointing accuracy.

10.2. Simulation Results

This section demonstrates the results of the Matlab simulations of the three PD controllers and assess their performance based on the accuracies achieved by them for large and small angle tracking rest-to-rest(regulation) maneuvers. PD controllers in Eq. 27 and Eq. 28 are simulated with Eq. 1 and Eq. 2 as the system, Eq. 12 as the gravity-gradient torque and $u_{\text{const}} = 1.18 * 10^{-3}$ N-m as the combination of SRP and constant external torque. The gains are tuned according to the insight provided in Table 6 [17], where k_d is greater than k_p in order to decrease the overshoot and settling times. For the twelve cases of simulation performed for three PD controllers listed in Table 7, $k_d = 8000$ and $k_p = 4000$ which are very high gains and is the downside of using PD controllers for such high accuracy missions. These gains can be lowered for small angle cases to achieve the 0.1 arcsec accuracies in three-spacecraft axes but for large angle slews, these gains are required to achieve approximately 0.1 arcsec accuracies in three-axes.

PD Gain	Rise Time	Overshoot	Settling Time	Steady-state Error
k_p	Decrease	Increase	NT(no definite trend: minor change)	Decrease
k_d	NT	Decrease	Decrease	NT
k_i	Decrease	Increase	Increase	Eliminate

Table 6 Characteristics of PD control corresponding to its gains.

Figure 24-Figure 26, Figure 27-Figure 29 and Figure 30- demonstrate the results of the simulation for linear PD controller in Eq. 27, Negative and Positive respectively NL PD controller in Eq. 28 for large and small angle maneuvers. In all the cases, accurate quaternion and angular velocity tracking is achieved as shown in Figure 24 using Linear PD for large and small angle reorientation, Figure 27 using Negative NL PD controller for large and small slew and Figure 30 using Positive NL PD controller for large and small angle maneuvers. Figure 25 shows the control torques applied to achieve quaternion errors of 0.02 and 0.05 arcsec respectively for large angle slews using linear PD controller. Figure 26 demonstrates the control torques applied to achieve quaternion errors of 0.02 and 0.05 arcsec respectively for small angle slews using linear PD controller. Results for analogous cases are shown in Figure 28-Figure 29 and Figure 31-

Figure 32 for negative and positive nonlinear PD controllers respectively. These results are listed in Table 7 which shows that small angle maneuvers require lesser input control torques as compared to large angle slews which is logical as more torque is required to reorient for large angles with the same high accuracies. This trend was seen in SMC and LQR in Section 8 and 9 and is similar for NL PD controllers case also.

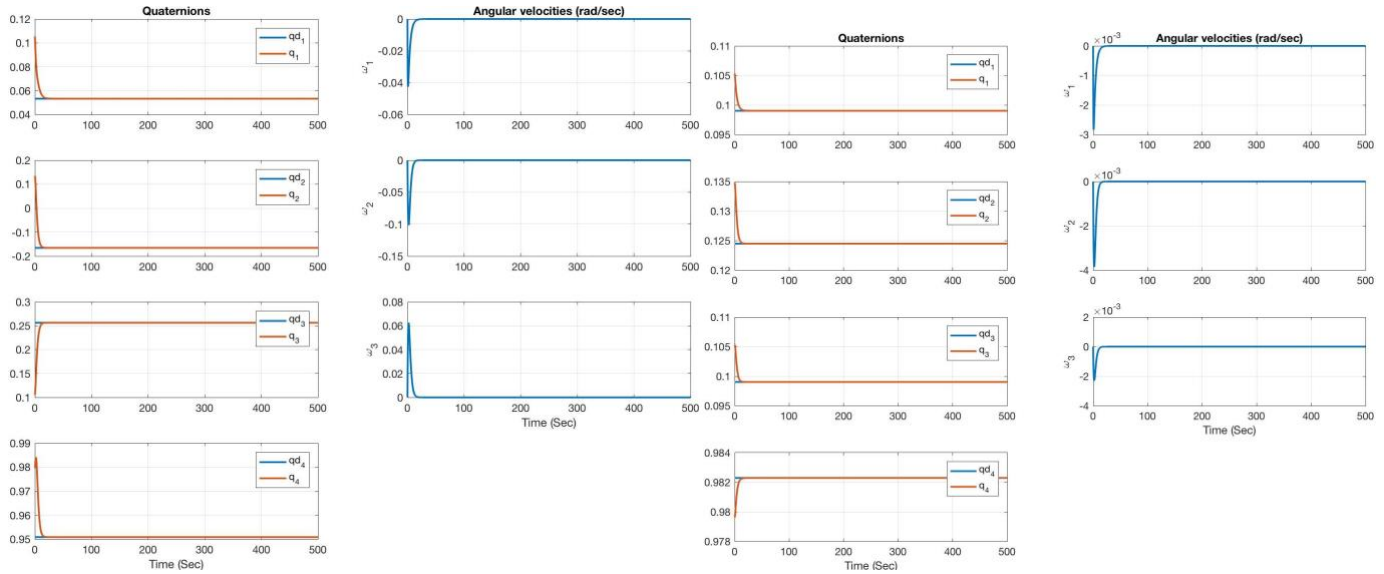


Figure 24 Linear PD: a. Large angle slew: Quaternion and Angular velocity Tracking b. Small angle slew: Quaternion and Angular velocity Tracking.

Table 7 lists the maximum control torques required to obtain pointing accuracies of 0.02 and 0.05 arcsec for large and small angle slews for all three PD controllers.

In summary, Table 8 compares the approximate maximum control torques calculated by all the five controllers namely SMC, LQR, Linear PD, Negative NL PD and Positive NL PD to obtain accuracy ≤ 0.05 arcsec. It thus validates the title of SMC as the highly accurate „the best controller in modern control theory“ because it applies the least amount of control torques to obtain the accuracies ≤ 0.05 arcsec. After SMC, PD controllers apply the second least control torques to obtain pointing accuracies ≤ 0.05 arcsec. Out of the three PD controllers, linear PD applies the least amount of torques for large angle slews which renders the two NL PD controllers moot as same accuracies can be achieved by the linear PD controller with lesser control torques. LQR applies the maximum torques of all the controllers for achieving accuracies ≤ 0.05 arcsec which is unexpected since it is a sub-optimal controller and should have performed better than PD controllers. Most likely reason of this is the way Riccati equation solution is calculated in LQR which is calculated using linearized spacecraft equations that does not represent actual nonlinear spacecraft equations. Comparing this to linear PD controller that is applied to nonlinear spacecraft equations although the controller itself is linear. Also note that the tuning parameters in all the five controllers are determined by trial and error which might also be the reason of this. Additionally, a constant control effort is required when using LQR as compared to SMC or PD controllers. Lastly, this table also validates our intuition that larger torques are required for large angle maneuvers as compared to small angle maneuvers (also validated in Table 4, Table 5 and Table 7). The control torques also increases when higher pointing accuracies are required, which is one of the main requirements of IRASSI mission and the main topic of discussion in this document.

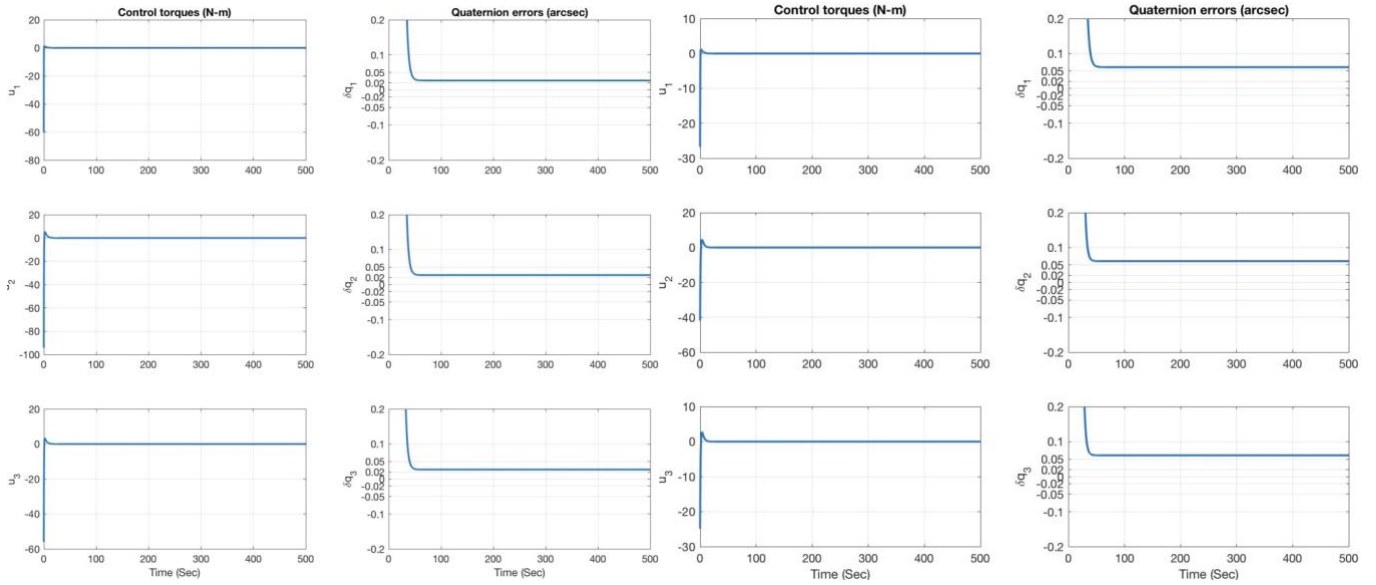


Figure 25 Linear PD- Large angle slew a. Control Torques when Quaternion errors~0.02 arcsec b. Control Torques when Quaternion errors~0.05 arcsec.

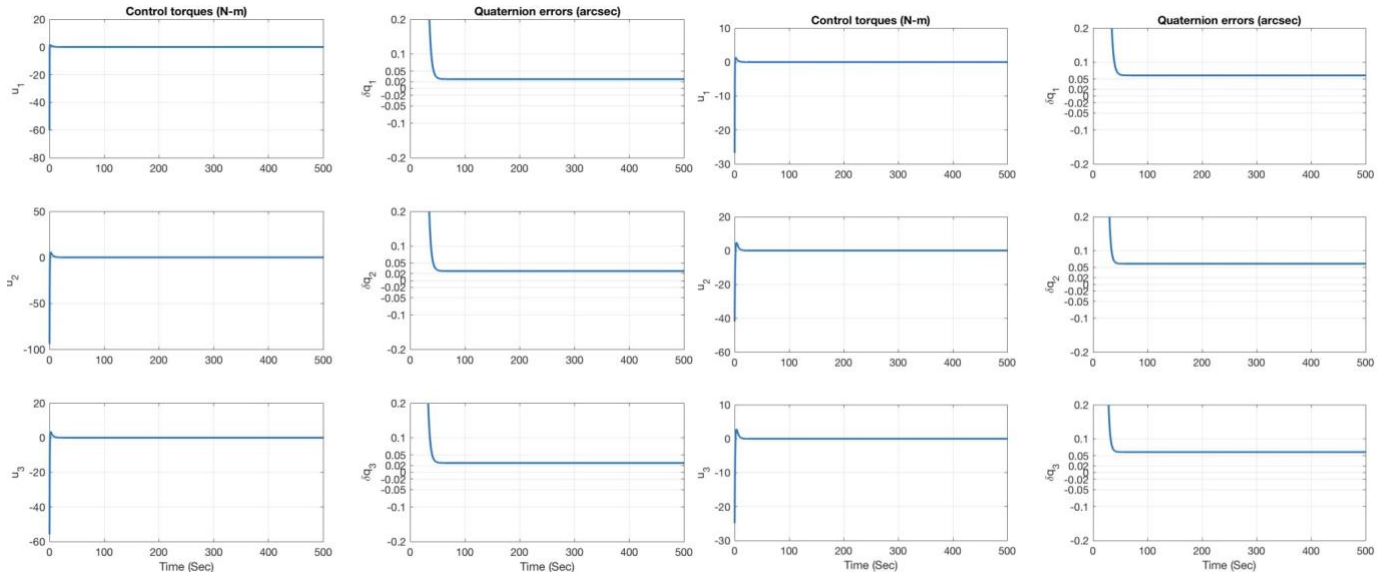


Figure 26 Linear PD- Small angle slew a. Control Torques when Quaternion errors~0.02 arcsec b. Control Torques when Quaternion errors~0.05 arcsec.

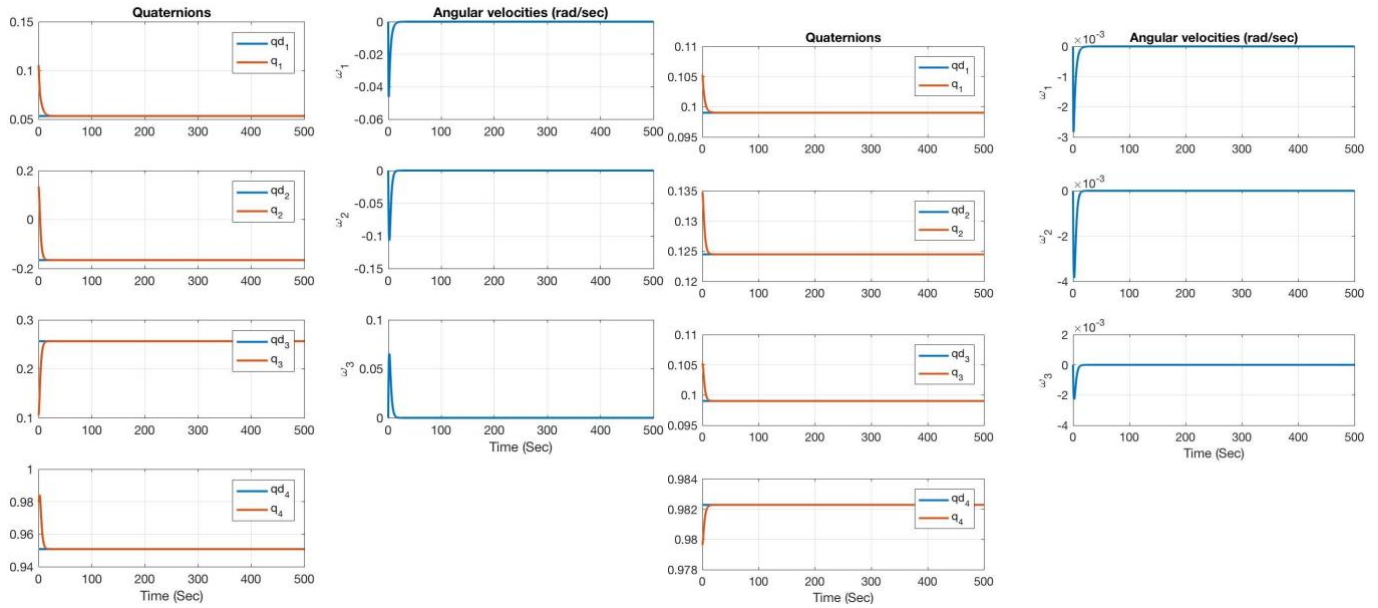


Figure 27 Negative NonLinear PD: a. Large angle slew: Quaternion and Angular velocity Tracking b. Small angle slew: Quaternion and Angular velocity Tracking.

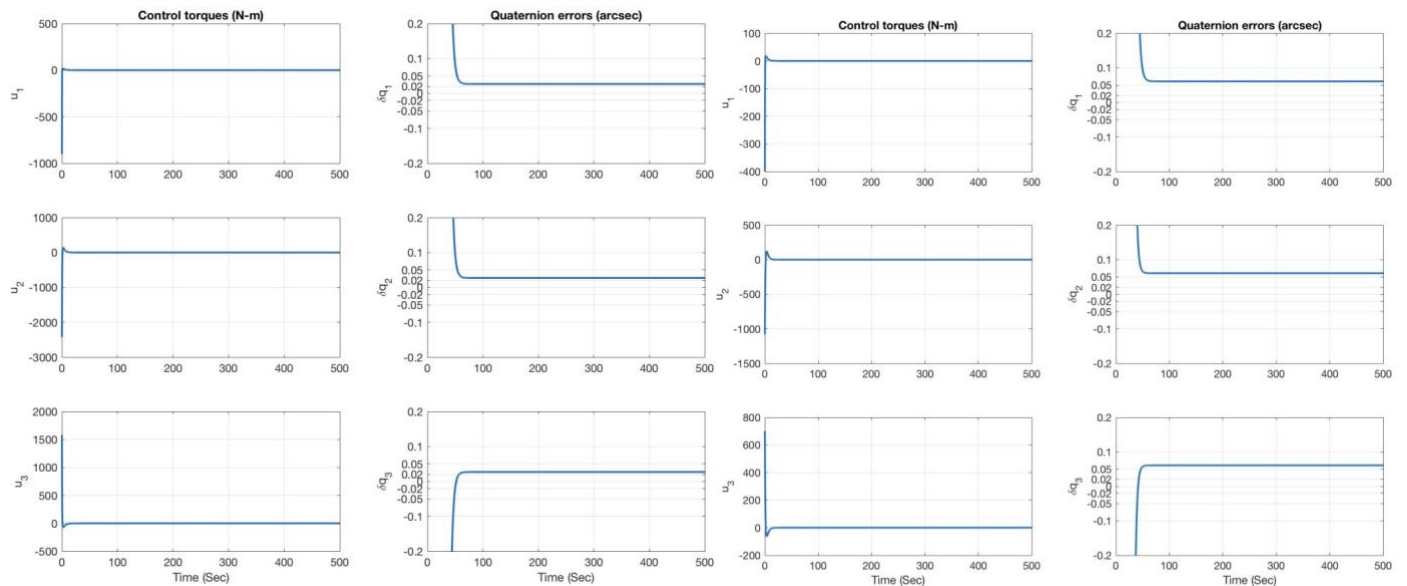


Figure 28 Negative Nonlinear PD- Large angle slew a. Control Torques when Quaternion errors~0.02 arcsec b. Control Torques when Quaternion errors~0.05 arcsec.

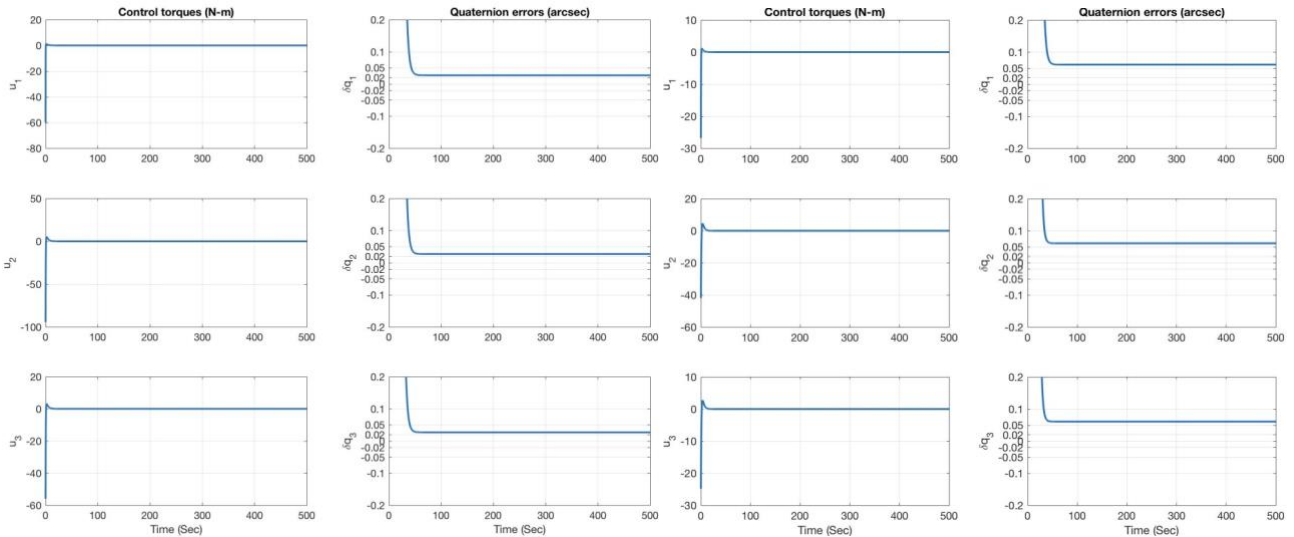


Figure 29 Negative Nonlinear PD- Small angle slew a. Control Torques when Quaternion errors~0.02 arcsec b. Control Torques when Quaternion errors~0.05 arcsec.

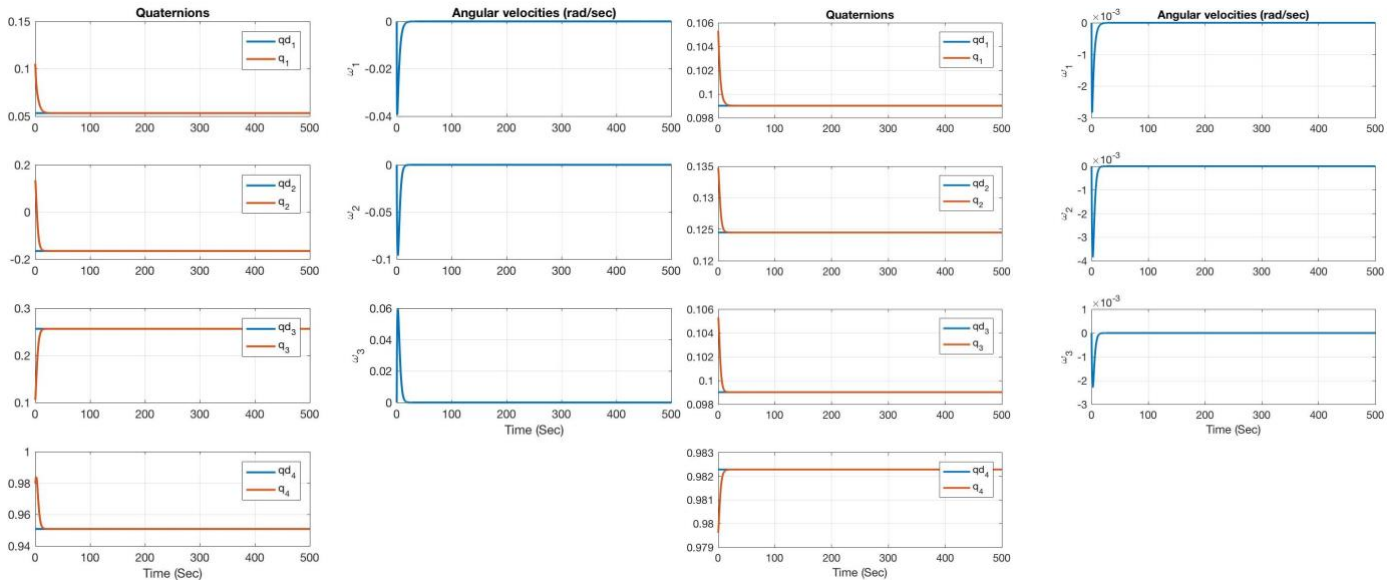
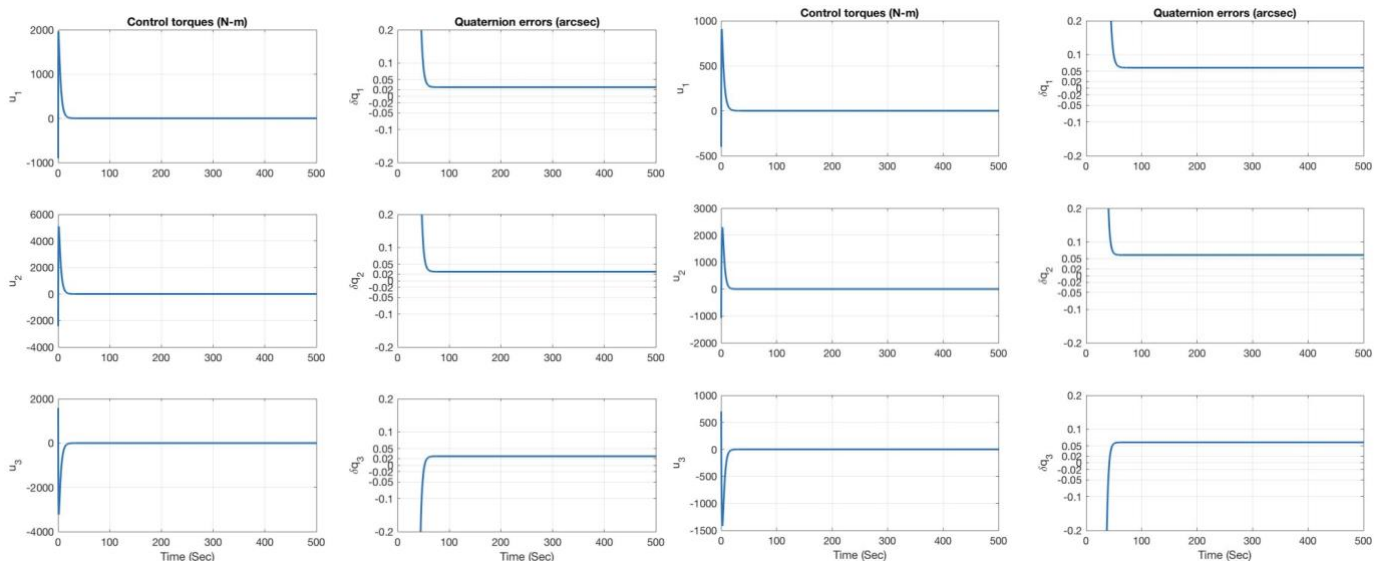
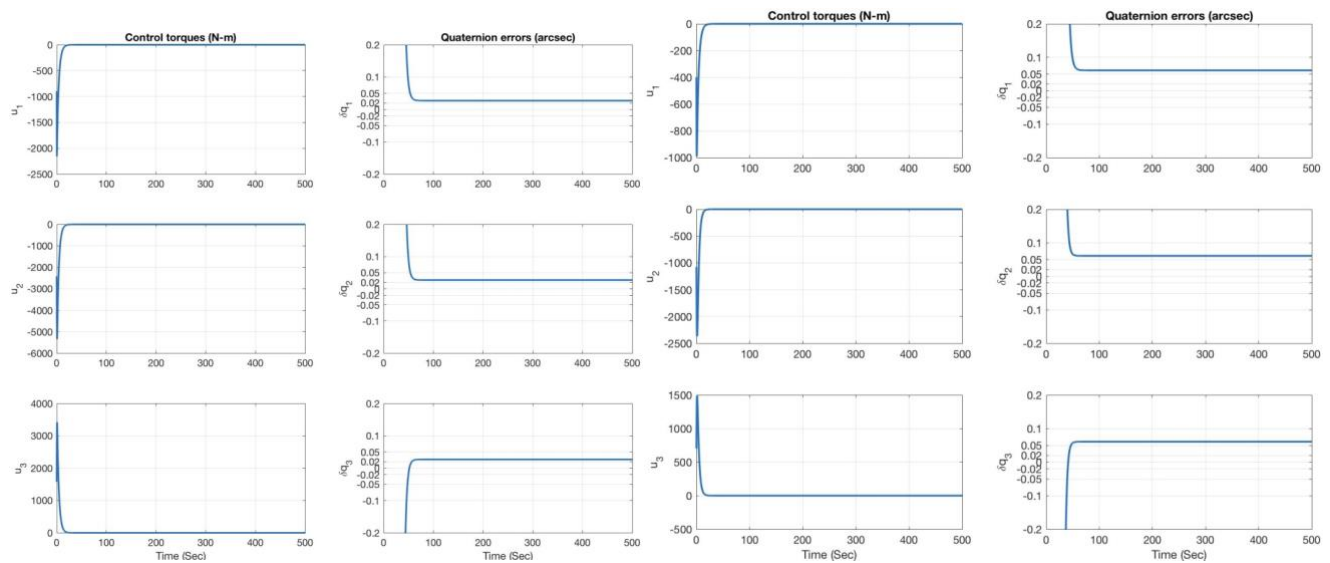


Figure 30 Positive NonLinear PD: a. Large angle slew: Quaternion and Angular velocity Tracking b. Small angle slew: Quaternion and Angular velocity Tracking.

PD Cases	Accuracy Achieved (arcsec)	Max. Control torque (N-m)
Linear PD: Large angle slew	[0.02,0.02,0.02]	[-60,-97,-56]
Linear PD: Small angle slew	[0.02,0.02,0.02]	[-60,-97,-56]
Linear PD: Large angle slew	[0.05,0.05,0.05]	[-26,-41,-24]
Linear PD: Small angle slew	[0.05,0.05,0.5]	[-26,-41,-24]
Negative NL PD: Large angle slew	[0.02,0.02,0.02]	[-900,-2400,1600]
Negative NL PD: Small angle slew	[0.02,0.02,0.02]	[-60,-97,-56]
Negative NL PD: Large angle slew	[0.05,0.05,0.05]	[-400,-1100,700]
Negative NL PD: Small angle slew	[0.05,0.05,0.05]	[-26,-41,-24]
Positive NL PD: Large angle slew	[0.02,0.02,0.02]	[2000,5200,-3200]
Positive NL PD: Small angle slew	[0.02,0.02,0.02]	[-2100,-5200,3500]

Positive NL PD: Large angle slew	[0.05,0.05,0.05]	[900,2400,-1400]
Positive NL PD: Small angle slew	[0.05,0.05,0.5]	[-1000,-2300,1500]

Table 7 Accuracies Achieved by Linear and NL PD controllers.**Figure 31 Positive Nonlinear PD- Large angle slew a. Control Torques when Quaternion errors~0.02 arcsec b. Control Torques when Quaternion errors~0.05 arcsec.****Figure 32 Positive Nonlinear PD- Small angle slew a. Control Torques when Quaternion errors~0.02 arcsec b. Control Torques when Quaternion errors~0.05 arcsec.**

Controller Type	Max. Control Torques N-m (Small Slew)	Max. Control Torques N-m (Large Slew)
SMC	[-3,-13,-8] for [0.05,0.02,0.02] arcsec	[40, 320,210] for [0.05,0.02,0.02] arcsec
LQR	[-1480, -1900,-1480] for 0.05 arcsec	[-1500, 2800,-4000] for 0.05 arcsec
Linear PD	[-26,-41,-24] for 0.05 arcsec, [-60,-97,-56] for 0.02 arcsec	[-26,-41,-24] for 0.05 arcsec, [-60,-97,-56] for 0.02 arcsec
Negative NL PD	[-26,-41,-24] for 0.05 arcsec, [-60,-97,-56] for 0.02 arcsec	[-400,-1100,700] for 0.05 arcsec, [-900,-2400,1600] for 0.02 arcsec,

Positive NL PD	[-1000,-2300,-1500] for 0.05 arcsec, [-2100,-5200,3500] for 0.02 arcsec,	[-900,2400,-1400] for 0.05 arcsec, [2000,5200,3200] for 0.02 arcsec,
----------------	---	---

Table 8 Approximate maximum control torques applied for achieving accuracies ≤ 0.05 arcsec by SMC, LQR and PD controllers.

11. CLOSED LOOP STABILITY OF NONLINEAR CONTROL ALGORITHMS

Work done in this section is carried out within sub-work package 5.2. Lyapunov's stability theorem [18], [5] is utilized to prove the stability of the above three controllers. There are two methods that provide the conditions of local and global stability of NL systems. First, 'Lyapunov Direct Method' for both linear and NL systems and second, 'Linear/linearized system stability conditions' for the linear/linearized systems as described below. Note that since the controllers analyzed in this document are discontinuous due to discontinuity of quaternions, the stability of these controllers as shown in sections 11.3-11.5 is a relaxed "almost" GAS in the sense of Lyapunov where asymptotic stability is defined over an "open" and dense set in SO(3). This means that these control algorithms provide local Asymptotic Stability in the sense of Lyapunov.

11.1. Lyapunov Direct Method

This is a general Method that provides global stability and is valid for both Linear and NL systems. Lyapunov (V) is closely related to the energy of a system, hence it is a scalar function. This method requires that Lyapunov should be Lipschitz. Lyapunov shows that when the system energy is dissipated, state is confined to volume bounded by constant energy surface such that system settles to equilibrium point. So, a system is Lyapunov stable where $V(x)$ is Lyapunov function if:

- $V(x_e) = 0$
- $V(x) > 0$ for $x \neq x_e$
- $\dot{V}(x) \leq 0$
 - If $\dot{V}(x) < 0$ for $x \neq x_e$, then x_e is AS (look at Section 11.2 for definition).
 - For $\dot{V}(x) \leq 0$, Lasalle's theorem [5], [18] is used to prove AS.

11.2. Linear/linearized system stability conditions

This method is valid for NL system's local stability around equilibrium points. Equilibrium point x_e is said to be Lyapunov stable if select bound on initial conditions results in trajectories that remain within chosen finite limit. x_e is Asymptotically Stable (AS) if $\lim_{t \rightarrow \infty} x \rightarrow 0$, where x is linearized state. x_e is

- Asymptotically stable (AS): (for NL system) if linearized system is strictly stable when eigenvalues of jacobian of NL system lies in the left half plane.
- Unstable: if linearized system is strictly unstable, atleast one eigenvalue of the jacobian of NL system lies in the right half plane.
- Marginally stable (MS): if atleast one eigenvalue of the jacobian of NL system lies on imaginary axis and the remainder lie in left half plane, which means that equilibrium point can be stable or unstable in this case and hence nothing can be concluded.

11.3. Nonlinear PD Stability Proof

Select a Lyapunov candidate function as [5]

$$V(x) = \frac{1}{4} \omega^T J \omega + \frac{1}{2} k_p q_{e1:3}^T q_{e1:3} + \frac{1}{2} k_p (1 - q_{e4})^2 \geq 0 \quad (27)$$

for equilibrium point $x_e = [q, w] = [0, 0, 0, 0, 1, 0, 0, 0]$. Hence $V=0$ for x_e . Taking the time derivative of Eq. 29 and substituting Eq. 2 and 4 in it gives

$$\begin{aligned}\dot{V} &= \frac{1}{2} \omega^T J \dot{\omega} + k_p q_{e1:3}^T \dot{q}_{e1:3} - k_p (1 - q_4) \dot{q}_4 \\ &= -\frac{1}{2} k_d \omega^T \omega \leq 0\end{aligned}\quad (28)$$

Hence the closed loop system (attitude kinematic and dynamics equations) with PD is Stable. Now, Lasalle can be used to prove its Asymptotically Stable (AS) as shown in [5]. The equality in Eq. 30 is given when $\omega = 0$ where $q_{e1:3}$ can be anything, i.e. $\lim_{t \rightarrow \infty} \omega = 0$. For AS, we have to check that the system remains in a state such that $\dot{V} = 0$ when $q_{e1:3} \neq 0$. The closed loop dynamics with Eq. 27 and 28 (one by one) in Eq. 2 shows that AS condition can be achieved if $\lim_{t \rightarrow \infty} q_{e1:3} = 0$. Hence, the three PD controllers provide closed-loop system asymptotic stability.

11.4. LQR Stability Proof

Select a Lyapunov candidate function as [15]

$$\begin{aligned}V(x) &= \frac{1}{2} \omega^T P \omega + q_{e1:3}^T q_{e1:3} + (1 - \delta q_4)^2 \geq 0 \\ P &= Q_{2,2}^{-1/2} R^{1/2} J\end{aligned}\quad (29)$$

where for equilibrium point $x_e = [q, w] = [0, 0, 0, 0, 1, 0, 0, 0]$

$$\begin{aligned}\dot{V} &= \omega^T J \dot{\omega} + 2 q_{e1:3}^T \dot{q}_{e1:3} - 2(1 - \delta q_4) \delta \dot{q}_4 \\ &= -\omega^T Q_{2,2}^{-\frac{1}{2}} R^{\frac{1}{2}} \omega \times J \omega - \omega^T Q_{2,2}^{-\frac{1}{2}} \left(Q_1 + \frac{1}{2} \left(J R^{\frac{1}{2}} Q_{2,2}^{\frac{1}{2}} + Q_{2,2}^{\frac{1}{2}} R^{\frac{1}{2}} J \right) \right) \left(Q_1 + \right. \\ &\quad \left. \frac{1}{2} \left(J R^{\frac{1}{2}} Q_{2,2}^{\frac{1}{2}} + Q_{2,2}^{\frac{1}{2}} R^{\frac{1}{2}} J \right) \right)^{\frac{1}{2}} \omega < 0\end{aligned}\quad (30)$$

LQR controller globally asymptotically stabilizes the nonlinear spacecraft system for any initial attitude. Hence from Eq. 32 and Lyapunov Theorem, closed loop system with LQR is AS [15].

11.5. SMC Stability Proof

For SMC, select a Lyapunov function candidate as [5]

$$V = \frac{1}{2} \sigma^2 \geq 0 \quad (31)$$

Taking time derivative of Eq. 33

$$\dot{V} = \sigma \dot{\sigma} \quad (32)$$

where

$$\dot{\sigma} = \dot{\omega}_e + \Lambda \operatorname{sign}(q_{e4}) \dot{q}_{e1:3} \quad (33)$$

Substituting Eq. 35 and σ in Eq. 34 gives

$$\dot{V} = -\sigma \operatorname{Gs}(\sigma_i, \varepsilon_i) \quad (34)$$

For positive definite matrix G , $\dot{V}(x) \leq 0$ [13]. To prove the AS, apply Lasalle as in [5] that proves that the system Eq. 1 and Eq. 2 are AS with SMC for equilibrium point x_e .

12. PERFORMANCE COMPARISON AND ANALYSIS OF CONTROL ALGORITHMS

The work in this section is carried out within work package 5.2. Although individual analysis of the three controllers, namely SMC, LQR and PD are provided in Sections 8-10, in this section we analyze them by comparing their performances. The metrics used for performance comparison are

- The accuracies achieved,
- Their global stability and
- Robustness towards disturbances, initial angles and large angle slews,

as shown in Table 9. Table 9 also lists two other details about these algorithms, i.e. the system used for the controller development and the type of controller. As shown in the table below, SMC achieves an accuracy ≤ 0.05 arcsec as validated by the simulation results in Section 8, is globally stable (validated in Section 11.5) and is robust towards disturbances, initial angles and large angle slews (validated in Section 8). SMC used for IRASSI is a nonlinear controller that controls the nonlinear spacecraft system shown in Section 8 and is the best controller for IRASSI's attitude control.

LQR achieves an accuracy ≤ 0.05 arcsec as validated by the simulation results in Section 9, is globally stable (validated in Section 11.4) and is robust towards disturbances, initial angles and large angle slews (validated in Section 9). LQR is a Linear controller that controls the nonlinear spacecraft system as shown in Section 9.

Control Method	Accuracy Required (arcsec)	Accuracy Achieved (arcsec)	„Almost“ Global Stability	Robustness			System Type	Control Type
				Disturbance	Initial angle	Large angle Slew		
SMC	≤ 0.3	≤ 0.05	Yes	Yes	Yes	Yes	NL	NL
PD		≤ 0.05	Yes	Yes	Yes	Yes	NL	NL and Linear
LQR		≤ 0.05	Yes	Yes	Yes	Yes	NL	Linear

Table 9 Performance Comparison of SMC, PD and LQR control design for IRASSI Spacecraft attitude tracking rest-to-rest maneuvers.

Linear and Nonlinear PD controllers achieve accuracies ≤ 0.05 arcsec as validated by the simulation results in Section 10, are globally stable (validated in Section 11.3) and are robust towards disturbances, initial angles and large angle slews (validated in Section 10). A linear PD and two Nonlinear PD controllers investigated for IRASSI are linear and nonlinear controller respectively all of which control the nonlinear spacecraft system shown in Section 10. It should also be noted that even though LQR and three PD controllers are robust towards the disturbances simulated for this analysis, these algorithms are inherently not robust towards disturbances unlike SMC.

13. SOFTWARE ENVIRONMENT FOR SPACECRAFT CONTROL IMPLEMENTATION

Matlab programming language executed on OS X operating system is used for the IRASSI spacecraft attitude control simulations demonstrated in previous sections. Figure 33 describes the general workflow diagram of the simulations for attitude control of IRASSI spacecraft. Three control algorithms, namely Sliding Mode Control, Linear-quadratic Regulator and Proportional-Derivative Controllers are implemented for Spacecraft rotational kinematic and dynamic equations which include the three external disturbances namely, gravity-gradient, solar-radiation pressure and constant torques as described in Section 7. The output parameters are the pointing accuracy, control torques, quaternions and angular velocity trajectories and others. The performances of these control algorithms are measured via accuracy achieved, stability and robustness characteristics where stability is established via Lyapunov theorem as explained in Section 11. Robustness of these algorithms towards external disturbances, initial conditions and large slew angles is also discussed in above sections. Results obtained with the simulation environment are described in the Sections 6-12 above.

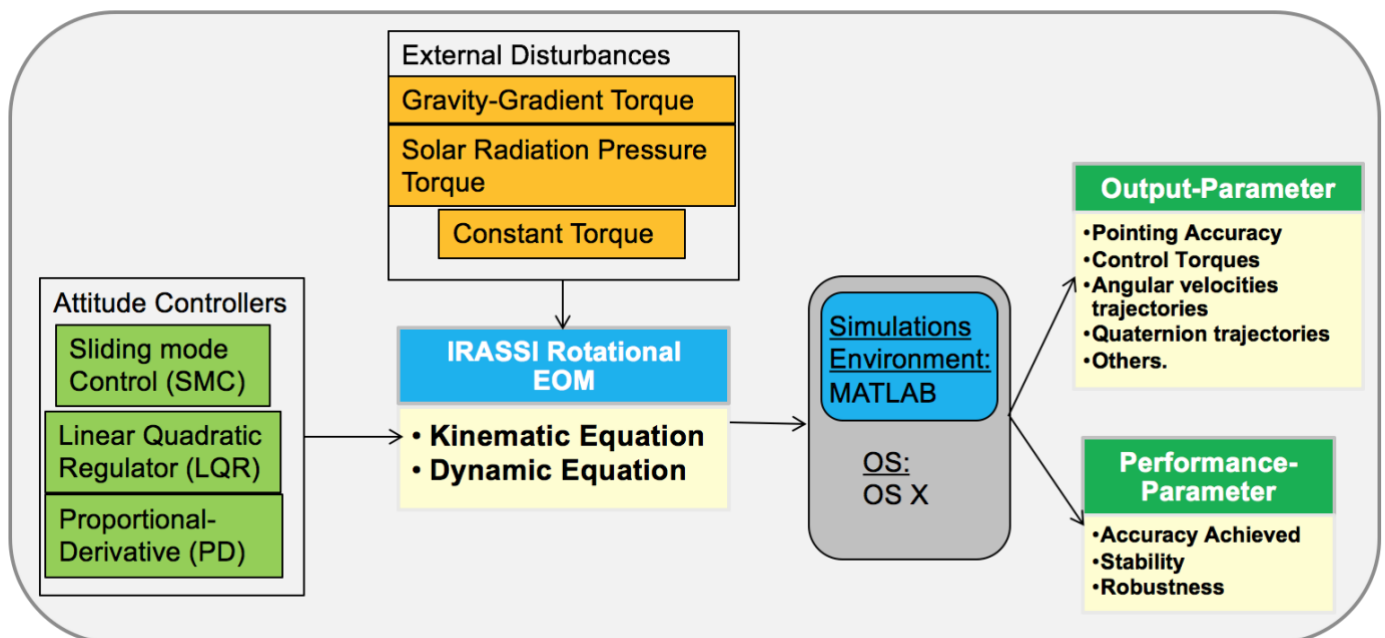


Figure 33 Architecture of MATLAB Simulation environment.

14. CONCLUSION

This document explains the research work performed by Institute of flight guidance (IFF) at Technischen Universität Braunschweig (TUBS) within "IRASSI". Within Work Package 5 titled 'Attitude Control System', IFF developed and designed three control algorithms for high accuracy pointing of IRASSI spacecraft, namely Sliding Mode Control, three Proportional-Derivative controllers and a Linear Quadratic Regulator. Out of these, three were nonlinear controllers (SMC and 2 PD controllers) and two linear controllers (one PD control and LQR). All these controllers are feasible for IRASSI stringent pointing accuracy requirement as they satisfy this requirement with flying colors. Then their stability and performance is investigated which shows that all of these controllers are globally stable and robust towards disturbances, initial conditions and large angle slews. These control designs are validated by the matlab simulations establishing their robustness towards disturbances, initial conditions and large slews. Their stability is established analytically via Lyaounov Theory. Table 8 compares the approximate maximum control torques calculated by these controllers to obtain accuracy ≤ 0.05 arcsec thus validating the title of SMC as the „best controller in modern control theory“ because it applies the least amount of control torques to obtain these accuracies.

Table 10 gists the pointing accuracies achieved by the attitude estimation system developed in IRASSI 1 and attitude control system developed in IRASSI 2 Phase 1, theoretically showing that a total pointing accuracy of 0.4 arcsec [1] for IRASSI satellite is possible. Table 11 lists the controllers that can be utilized for two mission modes defined in IRASSI 1, namely 1. **Fine Pointing Mode** during which science observations occur and that requires high pointing accuracies and 2. **Coarse Acquisition Mode** in which a coarse attitude of spacecraft is estimated with the help of sensors and estimation algorithms; and the spacecraft is maneuvered via actuators and control algorithms. Hence all five controllers investigated in this research are suitable for both these modes of IRASSI mission.

Spacecraft System	Accuracy Achieved (arcsec)	Total Accuracy Required
Attitude Estimation/Navigation (IRASSI 1)	0.03 (best-case) 0.1 (worst-case)	0.4 arcsec
Attitude Control (IRASSI 2 Phase 1)	0.02 (least in simulated cases) 2 (maximum in simulated cases)	

Table 10 IRASSI Spacecraft Pointing Accuracies Achieved By Attitude Navigation (IRASSI 1) and Control Systems (IRASSI 2 Phase 1).

IRASSI Mission Modes	Corresponding Attitude Controllers
Fine Pointing Mode	SMC, LQR and PD Controllers
Coarse Attitude Acquisition Mode	

Table 11 Controllers corresponding to the two IRASSI mission modes defined in IRASSI 1.

15. COOPERATION WITH PARTNERS

The result of IFF-TUBS (achieved attitude accuracy of 0.4 arcseconds) was used by AP3 and AP4 at the University of the Bundeswehr and by AP2 at the MPIA to carry out their work. The accuracy requirement of 0.4 arc seconds was derived from the scientific requirements established by MPIA.

16. APPLICATION

The three High accuracy Attitude Control Algorithms used and modified for IRASSI can be used for other space missions requiring such high accuracies, specifically other satellites operating in Halo orbit around Lagrange point 2 since they will also encounter the same external disturbances. These algorithms can be modified to include atmospheric drag for controlling attitude of any Earth observation satellites, for attitude control of aircraft, UAVs, ground-based system like cars and ship navigation. Hence, these algorithms are very generic and provide utility for widespread applications.

17. IMPLEMENTATION

One part of the results (as explained below) of TU Braunschweig within IRASSI were published in a conference paper and a bachelor thesis was supervised within IRASSI framework. In addition, the presentation of the results published in the conference paper was attended by various members of ESA and NASA, who attended the Astrodynamics Specialist Conference which led to the promotion of IRASSI. These implementations are shown below:

17.1. Publication

One part of the results of this document (i.e SMC method) was presented as part of the following paper at a space conference in USA, though the main topic and majority of the work in this paper is extra work because it was not proposed in the funded proposal.

- Divya Bhatia and Peter Hecker (August 2018). Disturbance-based High-Order Sliding Mode Observer-based Control for Spacecraft High Accuracy Pointing. AAS/AIAA Astrodynamics Specialist Conference, No. 367, August 19-23, 2018, Snowbird, Utah, USA.

17.2. Promotion of IRASSI to Space Agencies

Presentation of the above mentioned paper was attended by some members of NASA attending the above mentioned Astrodynamics Specialist Conference.

17.3. Students & Teaching

Within this project, a Bachelor thesis student was supervised as follows:

- Jinhao Liu, "Development and Analysis of Backstepping and Nonlinear Dynamic Inversion methods for Spacecraft High Accuracy Attitude control", Northwestern Polytechnical University, Department of Astronautics, Presented on 9 July 2018.

18. BIBLIOGRAPHY

- [1] H. Linz and S. Scheithauer, "IRASSI Science Requirement Specification: Derivation and Rationale," Max-Planck Institute of Heidelberg, Heidelberg, 2014.
- [2] D. Bhatia, U. Bestmann and P. Hecker, "High Accuracy Attitude Determination Estimation System for IRASSI interferometer Spacecraft," in *AAS/AIAA Space Flight Mechanics Meeting*, San Antonio, 2017.
- [3] D. Bhatia, U. Bestmann and P. Hecker, "High Accuracy Pointing Attitude Determination Estimator system for the future InfraRed Astronomy Satellite Swarm Interferometer," in *10th International ESA Conference on Guidance, Navigation and Control*, Salzburg, 2017.
- [4] D. Bhatia and U. Bestmann, "AbschlussBericht InfraRed Astronomy Satellite Swarm Interferometer-IRASSI 1," Technische Universitaet Braunschweig, Braunschweig, 2017.
- [5] F. L. Markley and J. L. Crassidis, *Fundamentals of Spacecraft Attitude Determination and Control*, New Jersey: Space Technology Library, Springer, 2014.
- [6] L. Buinhas, "Attitude Dynamics and Control at L2 of a single IRASSI Spacecraft," University of Bundeswehr, Munich, 2016.
- [7] E. Brucker and P. Gurfil, "Analysis of Gravity-gradient-perturbed rotational dynamics at the collinear Lagrange Points," *The Journal of Astronautical Sciences*, vol. 55, no. 3, pp. 271-291, 2007.
- [8] D. Bhatia, "Quaternions: Attitude Parameterization and Quaternion Algebra.," Internal IRASSI 1 Technical Document, Braunschweig, 2016.
- [9] U. Lee, *State-Constrained Rotational and Translational Motion Control with Applications to Monolithic and Distributed Spacecraft*, Washington: University of Washington, 2014.
- [10] O. Montenbruck and P. Gurfil, *Satellite Orbits: Models, Methods and applications*, Berlin Heidelberg: Springer Science and Business Media, 2012.
- [11] Y. Shtessel, C. Edwards, L. Fridman and A. Levant, *Sliding Mode Control and Observations*, New York: Birkhaeuser-Springer, 2013.
- [12] K. D. Young, V. I. Utkin and U. Oezguener, "A Control Engineer's Guide to Sliding Mode Control," vol. 7, no. 3, pp. 328-342, 1999.
- [13] J. L. Crassidis, S. R. Vadali and F. L. Markley, "Optimal Variable-Structure Control Tracking of Spacecraft Maneuvers," *AIAA Journal of Guidance, Control and Dynamics*, vol. 23, no. 3, pp. 564-566, 2000.
- [14] D. E. Kirk, *Optimal Control Theory: An Introduction*, New York: Dover Publications Inc., 1998.
- [15] Y. Yang, "Analytical LQR design for spacecraft control system based on quaternion model," *ASCE Library: Journal of Aerospace Engineering*, vol. 23, no. 3, p. 7, 2012.
- [16] R. M. Murray, *Control and Dynamical Systems Lecture 2- LQR Control*, California: Caltech, 2006.
- [17] Zhong, *PID controller tuning tutorial*, USA: Purdue University, 2006.
- [18] J. J. E. Slotine and W. Li, *Applied Nonlinear Control*, New jersey: Prentice Hall, 1991.
- [19] S. P. Bhat and D. S. Bernstein, "A topological obstruction to continuous global stabilization of rotational motion and the unwinding phenomenon," *Elsevier Systems and Control Letters*, vol. 39, no. 3, pp. 63-70, 2000.
- [20] J. B. Burl, *Linear Optimal Control: H2 and Hinfinity Methods*, California: Addison Wesley Longman Inc., 1999.

19. CORRECTION

This section informally publishes the errors in the official German translated Technical Report, with doi: [10.2314/KXP.1669390799](https://doi.org/10.2314/KXP.1669390799). These mistakes have been corrected in this English Technical report which was originally translated to German. Hence the mistakes in the official German technical Report and their corrections, along with the corrected mistakes in this English Technical Report are as follows:

Mistake and its correction in the official German Technical Report	Corresponding mistakes in this English Technical Report which was originally translated to German
<ol style="list-style-type: none"> 1. In Section 6, Nachteile, point II., line 7 should be "geodaetichse" instead of "nicht-geodaetichse". 2. In Section 7.2, the calculation of F_{SRP} is not correct. For correct calculation, refer to the section E. 1. of author's journal paper titled „Attitude Determination and Control System Design of Sub-Arcsecond Pointing Spacecraft“ with doi: 10.2514/1.G005116 3. In section 17.1, it should be „Ein Teil der Ergebnisse (d. H. SMC) wurde auf einer Weltraumkonferenz in den USA veröffentlicht:“, instead of „Die Ergebnisse wurden auf einer Weltraumkonferenz in den USA vorgestellt:“ 4. In section 17.2, it should be „An der Präsentation des oben genannten Papiers nahmen einige Mitglieder der NASA teil, die an der oben genannten Astrodynamics Specialist Conference teilnahmen.“, instead of „Die Ergebnisse wurden einer Raumfahrtagentur im Rahmen von dieser Konferenz wie folgt vorgestellt: Vorstellung der Ergebnisse bei der NASA im Rahmen der Astrodynamics Specialist Conference.“ 5. The order of the references in section 18 is jumbled. Please look at the correct order in this English document. 	<ol style="list-style-type: none"> 1. In section 6, Disadvantages, point 2, line 7, it is geodesic instead of non-geodesic. 2. In section 7.2, the wrong calculation of F_{SRP} is removed. 3. In section 17.1, the corrected sentence is „One part of the results of this document (i.e SMC method) was presented as part of the following paper at a space conference in USA, though the main topic and majority of the work in this paper is extra work because it was not proposed in the funded proposal“. 4. In section 17.2, the corrected sentence is „Presentation of the above mentioned paper was attended by some members of NASA attending the above mentioned Astrodynamics Specialist Conference.“. 5. Correct order of references is there in section 18 of this document.